

POLITECNICO DI TORINO

MASTER DEGREE IN ENERGY AND NUCLEAR ENGINEERING

MASTER THESIS

---

**Cell-based battery modeling to estimate the  
maximum power flexibility for a whole battery  
array**

---



*Supervisors:*

Prof. Enrico Pons

Prof. Mario Paolone, EPFL

*Student:*

Anna Irene Cavallo

October 25, 2018

# *Abstract*

In recent years, the penetration of renewable energy sources caused an increasing development of energy storage systems. In Smart Grids, these devices play an important role to supply power quality control in terms of voltage and frequency. They are essential also for shifting production and use of electricity. However, they are not able to tackle all types of requests but they can only work within the limit imposed by their maximum power flexibility. The main concern, as discussed in the thesis, is how accurately use batteries as energy storage systems. This will allow to operate the device avoiding system interruptions and will limit ageing phenomena take place, delaying the electrochemical material degradation. Experimental observations show the need to compute the device power flexibility by imposing boundary conditions at cell level, to be sure that no limit is exceeded. In effect, not all the cells within a battery pack have the same exact behavior.

The first part of the thesis is based on the study of different battery models, focusing on the grey-box model that will be implemented. The voltage prediction has been done by representing the battery with an equivalent electric circuit and solving it with a linearized equation derived from Kirchhoff's law. However, this type of model is not able to represent phenomena such as rate capacity effect, state of charge dependence and temperature influence on batteries behavior. In order to include all the nonlinear phenomena and make the model "robust" for any type of internal and external conditions, an adaptive method has been applied, the Kalman filter technique. It is able to correct the model estimates, by updating the model prediction with the last available measurements. In the second part, the predictor model is used to find the limiting power for a given battery state, derived imposing the cell limits in terms of current and voltage, and using an equation able to link the power to those variables. The thesis also faces with the estimation of the residual charge in the battery. It is complex to find because of internal losses and its dependence on temperature and current rate. In this sense, different models have been investigated.

The derived voltage predictor model has been applied to a real 25 kW / 25 kWh battery and the boundary conditions estimator tested in the EPFL experimental Microgrid. Some results of the state of charge estimation are given as well.

## *Abstract*

Negli ultimi decenni si è assistito ad una crescita sostanziale dell'utilizzo di fonti rinnovabili per la produzione di energia. La loro natura stocastica ed intermittente è la causa principale della ricerca di sistemi di accumulo adeguati, sostenibili ed efficienti. Tra i vari sistemi oggi presenti sul mercato, le batterie sono la tipologia più affermata grazie alla buona flessibilità di utilizzo, relativamente basso costo e buona integrazione nella rete, in particolare per eolico e fotovoltaico. Oltretutto, questo tipo di dispositivi è in grado di controllare la qualità dell'energia elettrica, in termini di frequenza e tensione. Tuttavia, non sono in grado di seguire ogni tipo di richiesta, ma sono caratterizzati da una massima flessibilità di potenza, che consente di rispettare i limiti di tensioni e corrente. Ciò permette di evitare interruzioni di servizio, limitare i fenomeni di invecchiamento e ritardare la degradazione dei materiali.

La tesi è incentrata sullo studio di diversi modelli capaci di prevedere il comportamento a breve termine di batterie, mostrando la necessità di imporre i limiti di utilizzo a livello delle singole celle che la costituiscono, a causa della loro inconsistenza in risposta ad una stessa eccitazione e stesse condizioni esterne. Il modello ritenuto più adeguato sarà applicato alle celle in condizioni più critiche e, con la previsione fatta, sarà possibile ricavare la flessibilità di potenza per il dispositivo nel suo complesso.

Il modello scelto è di tipo *grey-box*, basato sul classico circuito elettrico equivalente a due costanti di tempo. Il comportamento della batteria dipende da vari fattori, quali la temperatura di utilizzo, l'intensità di corrente, lo stato di carica. Nel nostro studio, assumiamo che la temperatura sia costante con buona approssimazione, in quanto siamo in presenza di un ambiente a temperatura controllata e il dispositivo è dotato di sistema refrigerante. Per rappresentare adeguatamente la dipendenza del modello da corrente e stato di carica, si è utilizzato un metodo ricorsivo, il filtro di Kalman, che utilizza l'ultima misurazione disponibile per aggiornare i valori dello stato interno del sistema e dare dei risultati più accurati, evitando che si verifichi un accumulo significativo dell'errore. Il modello è stato poi applicato a livello della singola cella per un dispositivo reale con caratteristiche nominali 25 kW / 25 kWh e testato con lo stimatore della potenza limite consentita nella Microrete sperimentale dell'EPFL nel Distributed Electrical System Laboratory (DESL).

La tesi è organizzata come segue: Capitolo 1 introduce i temi che verranno approfonditi nella tesi. Nel Capitolo 2 è presente una breve revisione della letteratura riguardo ai metodi di modellazione delle batterie. Nel Capitolo 3 sono approfonditi i metodi scelti in riferimento al dispositivo considerato. Il Capitolo 4 descrive la procedura utilizzata per l'implementazione del modello ed i risultati delle simulazioni e della validazione sperimentale nella Microrete. Infine, nel Capitolo 5 sono illustrate le Conclusioni del lavoro svolto.

# Contents

- 1 Introduction** **1**
- 1.1 Context and General Overview . . . . . 1
- 1.2 Experimental framework . . . . . 2
- 1.3 Goals and objectives . . . . . 2
  - 1.3.1 System identification . . . . . 3
- 1.4 Thesis structure . . . . . 4
  
- 2 Literature review of existing battery models** **5**
- 2.1 Basic principles of battery energy storage system . . . . . 5
  - 2.1.1 Battery non linear phenomena . . . . . 6
- 2.2 Review of existing battery modeling methods . . . . . 7
  - 2.2.1 Two Time Constant model . . . . . 9
- 2.3 SOC Estimation . . . . . 11
  - 2.3.1 Coulomb counting method . . . . . 12
  
- 3 Methodology** **14**
- 3.1 Implemented battery model . . . . . 14
  - 3.1.1 Preface and observations . . . . . 14
  - 3.1.2 Kalman-filter origins and definition . . . . . 15
    - Stochastic state-space mathematical models . . . . . 16
    - Kalman Filter algorithm: Rigorous mathematical formulation . . . . . 17
    - Kalman Filter implemented algorithm . . . . . 18
  - 3.1.3 Kalman filter technique - based model considering three time constants  
and variable voltage source . . . . . 18
    - Parameter identification . . . . . 21
    - The Pseudo Random Binary Signal . . . . . 21
- 3.2 Computation of the maximum power flexibility of the fully battery stack based  
on the cell-level model . . . . . 23
  - 3.2.1 Cell inconsistency problem . . . . . 23
  - 3.2.2 Formal computation of the battery cell active power constraint . . . . . 24
  - 3.2.3 Maximum power flexibility computation . . . . . 28
  
- 4 Implementation and Results** **30**
- 4.1 Experimental setup . . . . . 30
- 4.2 Definition and implementation of the experiments for the parameter identification 33
  - 4.2.1 Experiment assumptions . . . . . 33

4.2.2	The PRBS signal . . . . .	34
4.2.3	Parameter Identification . . . . .	35
4.2.4	Model simulation . . . . .	38
	Model error . . . . .	41
4.2.5	Model implementation using Kalman-filtering technique . . . . .	42
4.2.6	Maximum power flexibility computation . . . . .	45
	Result for charging mode at cell level . . . . .	46
	Result for discharging mode at cell level . . . . .	47
4.3	Experimental validation with the stack in the microgrid . . . . .	48
	Result for 2018.08.27 . . . . .	49
	Result for 2018.08.29 . . . . .	50
4.4	Discussion . . . . .	51
<b>5</b>	<b>Conclusion</b>	<b>53</b>
<b>A</b>	<b>Maximum power flexibility computation</b>	<b>55</b>
A.1	Matlab script . . . . .	55
A.2	LabVIEW code . . . . .	56
	<b>Bibliography</b>	<b>57</b>

# Chapter 1

## Introduction

### 1.1 Context and General Overview

Due to geopolitical and environmental issues, today renewable energy sources are increasing, since they seem to be the answer to hydrocarbons reduction in energy production. Especially regarding electric grid and transportation, these sources such as photovoltaic arrays and wind turbines are largely used, but still limited by their intermittent nature and reliability. This introduces issues of system stability, power quality and availability. To overcome the sporadic nature of renewable sources, energy storage systems are introduced to shift production and demand as far as possible. At the same time, these devices are able to ensure good power quality, by providing ancillary services to the grid, like voltage control and frequency support. Among all the available technologies, batteries and supercapacitors are very established and widespread. The first group is characterized by high energy density and relatively low power density, while supercapacitors have low energy density and high power density. Both batteries and supercapacitors need to work within a range of power limit, in order to avoid system interruptions or destruction of the materials and devices.

Due to their positive effect on energy management, power quality improvement and falling costs, batteries are very common in Smart Grid applications. Lithium batteries are very attractive because of their high energy density and very low costs. Furthermore, they are less toxic than others, like nickel cadmium or lead acid cells, and their disposal poses fewer environmental problems. Battery technology is growing up very fast, whereas the progress in both technology and materials cannot address all the concerns, such as costs, lifetime, environmental impact. Batteries as energy storage systems are buckly, just think about all the efforts to replace an old battery with a new one: you would like to avoid it until you can. Therefore, it is necessary to extend the devices operational life, for many reasons: less costs, since it saves purchase and disposal costs, lower environmental impact, etc. For doing that, one has to avoid and delay any damage of the device: all charge and discharge cycles have to be performed respecting all the constraints, usually expressed in terms of current, voltage and temperature limits. In effect, exceeding those values leads to faster ageing phenomena and over-exploitation of materials, reducing the battery life.

To achieve the power and energy value required by the user, several cells are connected in series or parallel. It should be noted that, in a battery pack, not all the cells have the same behavior under the same operating conditions. In the sense that, during normal operations,

each cell is characterized by different values of voltage, current and capacity, which is not visible controlling the global variables of the battery. To keep the device safe, since it is not sufficient to look at the total rack, the charge and discharge of each cell need to be monitored and controlled. Other types of batteries were quite tolerant to overcharge phenomena, such as lead-acid, nickel-cadmium. Moving to Lithium-ions, these events need to be avoided. In addition to all these concerns, we should not forget that it is essential to ensure a safe use of the battery, in order to integrate it correctly into the grid. In that respect, one has to guarantee an accurate control of the network, where the battery storage systems integration plays an important role.

For all these reasons, one needs to know for a given battery state which is the maximum charge/discharge power ensuring that limits are not violated, or in other words which is the maximum power flexibility. It will guarantee that the battery works in safe conditions, without giving any kind of alteration to the electrical grid, and preserving the state of the materials, to increase the battery life-time as much as possible. This job is usually carried out by the battery BMS<sup>1</sup>, which is responsible to control all the operations of the battery. However, typically it acts accounting for global variables, without considering the real cells behavior. To effectively use this kind of control, one needs to build a "boundary condition estimator" that applies current and voltage constraints at cell level to derive the limiting power values.

## 1.2 Experimental framework

The project takes place in the EPFL experimental Microgrid within the Commelec Framework. The lab work faces the challenge of controlling the electrical grid in real-time when it is characterized by a large penetration of stochastic generation, DC/AC converters, storage systems. In particular, the EPFL Microgrid is mainly powered by photovoltaic systems (peak power 50 kW) and a PEM fuel cell able to provide a 15 kW electrical output and 15 kW thermal output. The storage is allowed by a 25 kW / 25 kWh Lithium-Titanate battery array and a 75 kW / 2 kWh supercapacitor bank. The conventional approach for such a control involves a combination of voltage and frequencies control, but, with the increment of stochastic sources, it shows some limitations in terms of optimal and feasible operation of the network. The Commelec approach tries to break these limits based on the scalability and composability of the sources. It relies on an abstract representation of devices and subsystems, which are controlled by software agents which communicate with other agents, defining explicit and real-time set points in terms of active/reactive power defined by a solution of a specific optimization problem [1]. Within this context of electrical power systems, the availability of an accurate model for describing the dynamic behavior of the storage system is essential for model-based control of the grid.

## 1.3 Goals and objectives

The project deals with the study of battery modelling at the cell level in order to continuously estimate the short-term behavior of the device. This will allow to have a better estimation of

---

<sup>1</sup>BMS = Battery Management System

its maximum storage power flexibility. Very accurate battery models rely on the electrochemical dynamics happening inside the battery and are characterized by very high computational efforts and the need of expensive instrumentation for measurements. Black-box models, are essentially based on system input and output. They do not require any knowledge on the device working principle, though they can be unsuccessful. Among all the existing models, a grey-box model has been chosen for the implementation. This type of model gives the best compromise between computational costs and measurements availability required for the identification. It represents the battery cell by using an equivalent electric circuit, in which the parameters are resistances, capacitances, voltage generator, which need to be determined.

The complexity of the modeling procedure is due to the non-linear behavior of the battery: it depends on several features, such as temperature,  $C_{\text{rate}}$ <sup>2</sup>, State of Charge. As first assumption, we may not consider the temperature dependency, since the battery is equipped with a refrigerating system and kept at constant temperature. However, for taking into account the ageing phenomena effects and different operating conditions, it is essential to update the estimated parameters. For doing that, we chose to include in the model the Kalman filtering technique. It is a recursive method, relying on the last available measurements update, which is able, with it, to improve the model response. Recalling the cell inconsistency problem within a battery pack, 26 different sets of parameters have been identified, corresponding to the number of monitored cells. At each moment, the most critical cells are detected and then, the maximum charge power is computed in relation to most charged cell, while the maximum discharge power (later indicated also as minimum power for the sign convention used) with respect to the least charged cell. The reference to the "most" or "least charged cell" has to be understood in terms of voltage. In effect, we might refer also to the cell state of charge, but, as we will see, this is difficult to estimate because a unique definition does not exist. The ultimate goal of the project is the experimental validation of both the developed battery model and the boundary conditions estimator for the whole battery array in the EPFL Microgrid.

### 1.3.1 System identification

The model identification, most commonly indicated as system identification, consists of a process which allows to go from observed data to a mathematical model. The procedure is accurately described, for instance in [3, 4], and it requires four key components: observed data, one or more models, a criterion of fitting, validation.

1. *Observed data*: The input-output data are recorded during experiments dedicated to the identification. The user determines, if possible, the input signal type and which values have to be measured, in a way that the training data contain as many informations as possible. For instance, in our case a Pseudo Random Binary Signal (PRBS) has been applied because it is able to excite a wide range of internal dynamics.

---

<sup>2</sup> $C_{\text{rate}}$  is a measure of the rate at which a battery is discharged relative to its maximum capacity. A 1  $C_{\text{rate}}$  means that the discharge current will discharge the entire battery in 1 hour [2]. It is the ratio between the actual current and the nominal value.

2. *One or more models*: This is the most difficult choice, because the more accurate the model is, the more difficult and expensive (from both computational and economic point of view) is to determine it. As people often do, we chose the best compromise: a grey box model, which ensures acceptable results and fast and straightforward implementation.
3. *A criterion of fitting*: Fitting models to data is fundamental to extract useful informations from observations. Some of the methods are the Maximum Likelihood Estimator (MLE) or Prediction Errors Minimization (PEM). For this step the *greyest* Matlab function has been chosen to extract the parameters. It performs several iterations, using for each of these the technique associated to the lowest computational effort.
4. *Validation*: It is the last step which consists in testing whether the model is valid to its purpose. A "good" predicting model implies that it is accompanied by small prediction errors. It is sufficient to run the model in real-time and to compare it to the actual data.

## 1.4 Thesis structure

The thesis is organized into five chapters: 1) Introduction, 2) Literature review of battery existing models, 3) Methodology, 4) Implementation and results, 5) Conclusion. Chapter 2 contains a brief literature review of the battery existing models, distinguishing between *white-box*, *black-box* and *grey-box* models. Then, it focuses on this last listed item, especially on equivalent electric circuit models. Chapter 3 studies more in detail the model that will be implemented and then tested in the Microgrid. It focuses on the theoretical aspects to get everything we need for the practical applications. It also accurately describes all the steps necessary for the system identification. Chapter 4 is dedicated to the implementation of the model on a real battery. It basically turns all the equations derived in the previous chapters into codes, numbers, plots. It also contains some results relative to the model simulation and the experimental validation in the Microgrid. Finally, Chapter 5 presents an overall comment on the work that has been done, especially on the results and possible future works.

## Chapter 2

# Literature review of existing battery models

### 2.1 Basic principles of battery energy storage system

Although in this section sometimes is explicitly specified "Lithium-ions" batteries, since it is the type of battery we will work with, the principle illustrated is valid for other types of batteries. The operating principle of batteries relies on the internal chemical kinetic process. In fact, Lithium-ions batteries consist in a structure of cathode and anode, which are the electrodes, and electrolyte. During each discharge/charge process, lithium ions are continuously exchanged from one electrode to the other passing through the electrolyte. Their insertion/extraction into/from the electrode material creates a series of redox reactions accompanied by a flow of electrons through the external circuit. During charge and discharge phases, the layer structure is preserved, enabling the reversibility of the process [5]. Charging the battery connecting it to an external source, the infinite charges are stored in the electrolyte. Instead, connecting the battery to an external load, the stored charge is generated through the external circuit and the battery discharged. One can assume that the potential difference across the device terminals makes that the charges form several layers in the electrolyte. This property is introduced by Manwell in 1993 in [6]. He was the first one to consider that in the cell electrolyte there are several layers where the charges are passing through (see Fig. 2.1a).

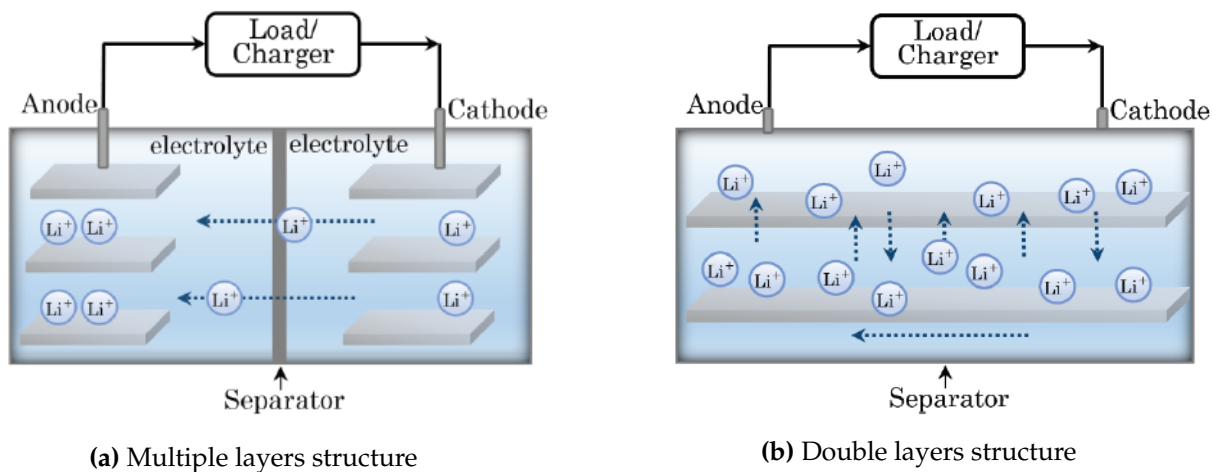
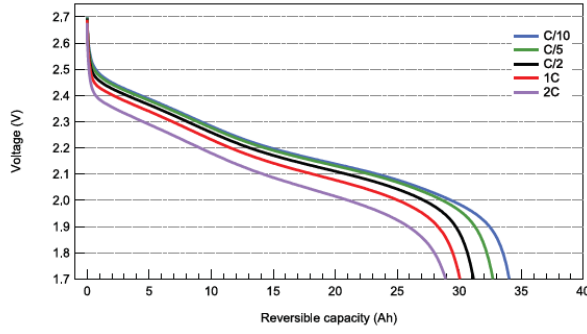
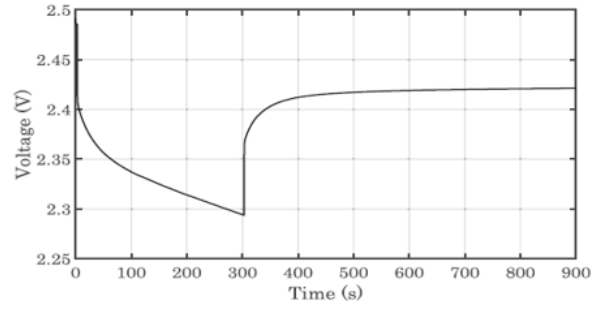


Fig. 2.1. Structure of the lithium-based battery cell electrolyte [7]



(a) *Rate capacity effect.* Evolution of the Reversible cell capacity for different  $C_{rate}$ . The capacity increases at high  $C_{rate}$  [9]



(b) *Recovery effect.* At time  $t=300s$ , the load is disconnected and part of the charge is restored. Consequently, there is a voltage drop causing an increment of it. [7]

Fig. 2.2. Battery non linear effects

All these layers can be grouped as two main layers or tanks as in Fig. 2.1b: one is the "available" tank, constituted by the surface layers and it holds charge that is immediately available to be used by the load. The other tank is constituted by the "bondend" charge, represented by the inner layers and holds charge that is chemically bound, acting as storage reservoir and exchanging charges only with the surface layer. The charges exchanged between these layers are the major responsible of the nonlinear behavior of the battery.

### 2.1.1 Battery non linear phenomena

As already mentioned, batteries are characterized by non-linear behaviours for their intrinsic nature, as they provide power and energy storage based on electrochemical mechanisms. The main responsible is the charge exchanged between the inner and surface layer, but it is not only one. In effect, batteries non-linearity is represented by three main phenomena [7, 8]: rate capacity effect, recovery effect, hysteresis effect, temperature dependence.

The *rate capacity effect* consists in the fact that the amount of charge one can extract changes according to the load current. It makes that the charge you can extract at low current is always higher than the one deliverable at higher current. A plausible explanation is that the charges in the storage tank do not have time to reach the available layer. In this regard, Fig. 2.2a is provided by the manufacturer in the technical data sheet. The extractable capacity for increasing  $C$  is illustrated, where 1C corresponds to the cell nominal current. That is the proof the capacity increases as soon as the current decreases. Clearly, it emerges that the behavior is not linear. Furthermore, it is subject to change over time.

*Recovery effect:* it is noticeable when the battery is disconnected from a load/charger, during the so called "relaxation phase" (or "resting phase"). While discharging, charge migrates from the storage to the available tank. As soon as the charge stop going to the external system, there is a certain amount of charge that has not been extracted but it is still present in the available tank. This quantity will migrate from the outer to the inner layer, creating an increment of the

battery terminal voltage. On the contrary, disconnecting the battery from a source, it causes a decrement on the terminal voltage, because the charge in the inner layer goes to the outer layer to keep the equilibrium of the system. The voltage trend is represented in Fig. 2.2b, for the case of disconnection from a load. In the case of disconnection from a source, the curve is reversed.

*Hysteresis effect* is represented by the fact that, given a value of state of charge, the charging voltage curve is always above the discharging voltage curve.

Also the temperature plays an important role, influencing also the described effects. Experimental observations show that, in discharging phase, the voltage at low temperature reaches lower final value with respect to the same battery at higher temperature. During charging, the higher the temperature the more the time required to reach the same final voltage. Indeed, it seems that the temperature does not effect the open circuit voltage. In Fig. 2.3 the results obtained in [7] are illustrated as example for experiments at 25, 35, 45, 55° C.

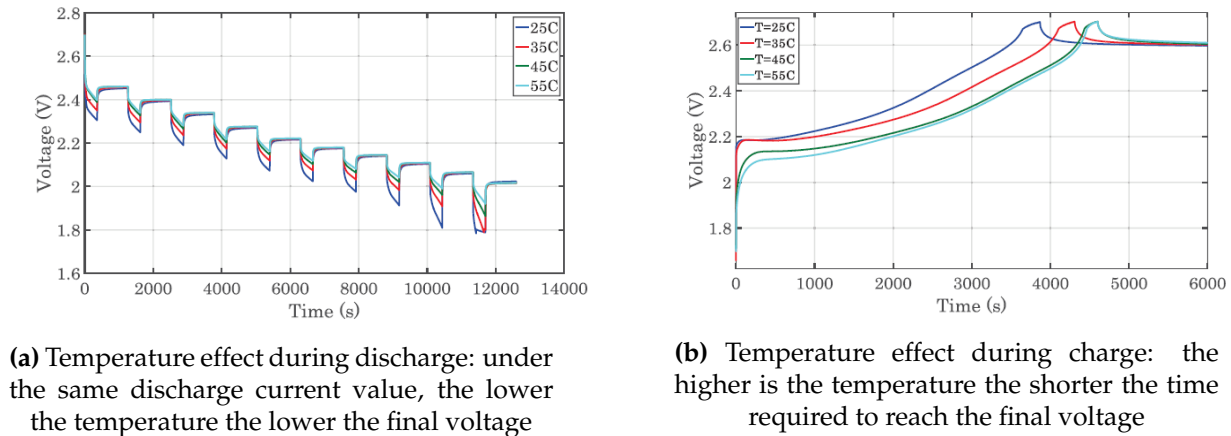


**Fig. 2.3.** Temperature influence on battery cell voltage from experimental results in [7]

## 2.2 Review of existing battery modeling methods

A battery model is a instrument able to predict the device output/s, given one or more input. For our discussion, the input is the current, while the model output is the battery voltage. An accurate battery model is crucial for monitoring and control the battery, in order to properly handle charge and discharge cycles, as well as for estimating key factors such as the state of charge. In effect, this last parameter is not directly measurable, hence, it can just be estimated by having a model. To ensure safe and efficient operation, a proper battery model is essential to predicting battery behaviour under various operating conditions, in order to avoid improper operations, like over-charging and over-discharging. However, the dynamic behaviour of batteries is extremely difficult to model due to highly non-linear dynamics, caused by complex internal electrochemistry reactions. The study of the literature concerning battery modeling allows to identify three main categories of models to estimate the complex nonlinear voltage-current behaviour, having different level of complexity and accuracy: white-box models such

as electrochemical model, grey-box models such as equivalent electric circuit models, as well as black-box models such as neural network models [10, 11].

### 1) *White-box model*

It comes out from microscopic observation of the battery cell. Talking about lithium-titanate battery, it is based on the lithium ions diffusion through the cell structure. During discharge, Li-ions diffuse between the surface of the negative and the positive electrode, where they react and transfer to an electrolyte solution. The positively charged ions travel through the electrolyte solution via diffusion and migration. When electrons are produced in the negative electrode reaction, they travel through an external circuit. Such a model describes the electrochemical processes taking place within the battery cell, relying on detailed mathematical tools, made of complex nonlinear differential equations. Charge and discharge cycles are modeled based on the concentrated solution theory, or, more precisely, on the electrochemical reactions in active solid particles in the electrodes and on the mass transport mechanism of Lithium-ions across the electrodes. It is able to predict solid-state and electrolyte diffusion dynamics, providing a good current-voltage response, but it requires differential equations to be solved through numerical methods. It is the most accurate model although it requires detailed description of the chemical processes, expensive instrumentation and highly computational costs. This kind of model provides meaningful informations about the battery internal state, however, the computational complexity is far beyond the BMS hardware capability. It means that these models cannot run in real-time and, therefore, are not usable to our purpose. Several approaches of electrochemical battery models simplification have been proposed but they are still too complex to be used in a BMS [12, 13, 14, 15, 16].

### 2) *Black-box models*

They describe battery behaviour using some intelligent modelling methods, without the need to understand the electrochemical processes occurring in the battery. This kind of model is free of any information about battery type and structure. To approximate the non-linear voltage-current curves, they use nonlinear regression models such as Radial Basis Function Networks (RBF) or Teaching-Learning-Based Optimization (TLBO). The RBF considers a multiple inputs single output system (MISO), in which the output has a relatively simple mathematical formulation with an arbitrary number of parameters. The key issue is still the need of a powerful mean to have an optimal assessment of the parameters. TLBO is a nature-inspired population based optimization algorithm. It is divided into two parts: the teacher phase, where the learners learn from the teacher to improve the grades, and the learner phase, in which learners learn from the interactions between themselves. If, on one hand, extracting the parameters of the mathematical functions from the voltage-current characteristics results in fast computation models, on the other hand, these models do not allow direct variations of the parameters following a system change. They would need to repeat all the measurements needed for parameterizing the model. Some example of black-box model application are given in [11, 17, 18].

### 3) *Grey-box models*

It is a kind of empirical models which aim at abstracting the physical phenomena taking place

inside the battery cell, by using a combination of voltage and current sources, capacitors and resistors. It basically uses equivalent electric circuits, in which the parameters are obtained by experimental tests. However, most of these identified parameters have little reflect to the real physical parameters of the battery. There are many electrical models of batteries, which can be grouped in three basic categories: Thevenin-based, impedance-based and runtime-based models. [7, 19, 20, 21]

- Runtime-based models use a complex circuit network to simulate battery runtime and voltage response. The estimation is accurate for constant discharge current but they can not predict runtime nor voltage response for varying load currents accurately.
- Impedance-based models employ the method of electrochemical impedance spectroscopy and then use a complicated equivalent network to fit the impedance spectra. The fitting process is therefore difficult and complex.
- Finally, a Thevenin-based model, in its most basic form, uses a series resistance and a resistance/capacitance parallel branch to predict battery response. Such a model is basically empirical and it depends on a set of parameters that need to be estimated from experimental measurements.

### 2.2.1 Two Time Constant model

As results of the discussion just made, we focus in this section on electric circuit models. They exhibit the best tradoff among accuracy, computational costs and data availability. Furthermore, they present straightforward implementation, also because circuits are very familiar and intuitive in electrical engineering field. The most common available model in this context is the Two Time constant (TTC) model. It is a type of grey-box model, representing the battery behavior according to physical knowledge of the system and real measurements. It considers battery dynamics happen following two time constants: "fast dynamics" and "slow dynamics". It includes a voltage source representing the open circuit voltage, a series resistance accounting for charge/discharge losses, and two branches containing a resistance and a capacitance in parallel to describe the slow and fast electrochemical processes during charge and discharge, as well as during redistribution phases. It is shown in Fig. 2.4, where the parameters can be described in detail as follows:

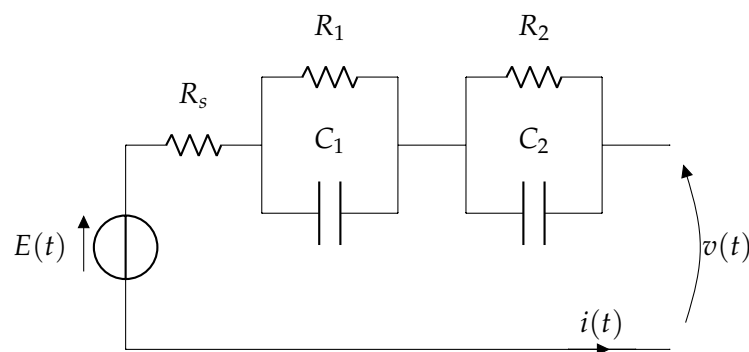


Fig. 2.4. Equivalent electric circuit for TTC battery model

$R_s$  is the battery series resistance which is used to take into account the energy losses of the battery cell during charge or discharge operations. It is the cause of a voltage drop during operation and also dissipates useful energy as waste heat. This effect is usually considered as 'polarisation' and is function of the current intensity.

$C_1, R_1$  are respectively the capacitance and the resistance of the first branch. They model the fastest electrochemical dynamics;  $C_1$  characterizes the transient response of charge transfer between the two layers and the accumulation of the charges before polarizing and diffuse between electrode and electrolyte.  $R_1$  represents the energy losses due to the charge transfer within the double layer.

$C_2, R_2$  are the resistance and the capacitance of the second branch respectively. They model the slowest electric dynamics.

$E$  is the open circuit voltage, the equilibrium electromotive force which can be measured as voltage across the circuit terminals under no load conditions.

The circuit in Fig. 2.4 is solved by applying the Kirchhoff's laws. One can write:

$$\begin{cases} v_1(t) = [v_1(t_0) - R_1 i(t)] e^{-\frac{t-t_0}{R_1 C_1}} + R_1 i(t) \\ v_2(t) = [v_2(t_0) - R_2 i(t)] e^{-\frac{t-t_0}{R_2 C_2}} + R_2 i(t) \\ v(t) = E(t) + R_s i(t) + v_1(t) + v_2(t) \end{cases} \quad (2.1)$$

where  $v_1$  and  $v_2$  are the voltage drops across the two RC branches. To sum up, the terminal voltage is presented in Eq. 2.2, where  $R_s, R_1, C_1, R_2, C_2, E$ , is the set of parameters to estimate:

$$v(t) = E(t) + (R_s + R_1 + R_2) i(t) + [v_1(t_0) - R_1 i(t)] e^{-\frac{t-t_0}{R_1 C_1}} + [v_2(t_0) - R_2 i(t)] e^{-\frac{t-t_0}{R_2 C_2}} \quad (2.2)$$

For the sake of simplicity and subsequent applications, more often a simplified linearized model is used. It is derived by approximating the exponential term with its Taylor series representation. The main advantage is that, using this formulation, a state-space model can be derived, expressing it as a function of two state space variables  $v_1(t)$  and  $v_2(t)$ . The input is the current  $i(t)$ , whereas the output is the voltage  $v(t)$ . It is given in the following equation (2.3), where the time dependency is omitted to make it clearer:

$$\begin{cases} \dot{x} = Ax + Bu \\ v = Cx + Du \end{cases} \quad (2.3)$$

where  $v$  is the model output (battery terminal voltage),  $x$  system state vector,  $A$  the transition matrix,  $B$  is the input system matrix,  $C$  the measurement input matrix,  $D$  the feedforward matrix,  $u$  input vector.

The system state vector  $x$  is a modelling abstraction of the phenomena happening inside the battery, and thus not measurable. Its expression is mentioned below in (2.4) together with the

other terms of the state-space formulation:

$$x = \begin{bmatrix} v_{C_1} \\ v_{C_2} \end{bmatrix} \quad u(t) = i(t)$$

$$A = \begin{bmatrix} -\frac{1}{R_1 C_1} & 0 \\ 0 & -\frac{1}{R_2 C_2} \end{bmatrix}, \quad B = \begin{bmatrix} \frac{1}{C_1} \\ \frac{1}{C_2} \end{bmatrix}, \quad C = [1 \quad 1], \quad D = [R_s \quad E] \quad (2.4)$$

where  $R_1, R_2, C_1, C_2, R_s, E$  is the set of parameters to be estimated.

In order to take into account the nonlinear effects already described in section 2.1, we should consider the parameters dependency on the battery SOC, temperature and  $C_{\text{rate}}$ . Often batteries are equipped with refrigerating systems, therefore the temperature can be considered constant in time. The SOC dependency is accounted for by building several models, keeping the battery in different SOC ranges. Each model presents different parameter values, which can be organized in look up tables. The  $C_{\text{rate}}$  dependency is more difficult to model. Several adjustments have been tried in this sense. For example, in the model proposed in [7], it is addressed through a virtual current generator which is activated when the  $C_{\text{rate}}$  is different from the one used for parameters assessment, in order to account for the different amount of charge being redistributed.

## 2.3 SOC Estimation

Talking about battery modelling, State of Charge estimation is one of the main concerns. A precise SOC estimation of the battery is essential for ensuring a proper use of the device and it also represents the easiest way to avoid any unwanted system interruption. It is also needed to preserve the material which can be compromised by an inappropriate use, such as involving overcharging and overdischarging phenomena. These events may cause quick and permanent damages to the battery internal structure. If on one hand the SOC estimation is a key factor for correct and safe battery management, on the other hand a unequivocal SOC definition does not exist. The battery state of charge is physically related to the quantity of solide particles concentration at the electrodes [22]. Actually, the effective extractable charge is always lower than the available one. In fact, there are some losses during charging and discharging operations, as explained in section 2.1.1. Furthermore, this quantity is not easy to measure in real-time application, hence, the SOC is more often indirectly estimated from other measurable quantities. Different models have been proposed with the goal of improving the results [7, 23, 24, 25]. They are recalled hereafter.

- i. *Open circuit voltage algorithm*: It is a simple way to estimate the SOC, relying on appropriate look-up tables containing the relationship between open-circuit voltage and state of charge. A number of points is taken in the feasible voltage values range, and for each of them the open circuit voltage is recorded after the relaxation phase has taken place. Then, the battery is discharged and the extracted charge measured by integrating the current over the time. With this second value, the table can be built point by point. The implementation is simple, but in order to reach the open-circuit voltage, long time is needed

after the load is removed. This method is not accurate in real-time operation since the system is far from no load conditions.

- ii. *Coulomb counting method*: It defines the SOC as the amount of available charge over the maximum charge. Hence, it depends on a quantity that, in turn, is difficult to estimate. In fact, the nominal capacity is also function of the current, besides the temperature. In addition, it requires an initialization which has to be as precise as possible. For these reasons, as well as for possible measuring instrument inaccuracies, it is not very precise and characterized by accumulating error.
- iii. *Algorithm using Electrochemical Impedance Spectroscopy (EIS)*: It relies on the impedance measurement, whose value largely depends on the adopted method, and it is very sensitive to measurement conditions as well. Moreover, the relationship between the electrochemical impedance and the SOC is not unique and depends on the type of battery. It requires dedicated expensive hardware and results difficult to implement in real-time application.
- iv. *Artificial Neural Networks (ANN)*: This group of methods gives quite accurate results but the computational complexity is very high. Furthermore, to improve the model accuracy, they require a large number of offline data. Therefore, it may take considerable time to entirely define the model.
- v. *Model-based filtering methods*: They count on the use of filter to have a better estimation of this variable, but still using another model as starting point. For example in [22], the SOC computation is based on a electrochemical simplified model, corrected by using Kalman filtering technique (in section 3.1 there is a in-depth study of the Kalman filter). It gives good estimation results, but it requires detailed expensive measurement and high computational efforts, typical of white box-models. In this context, the same technique has been applied, for example, to an electric circuit based model, proposed by Plett in [26]. It includes the SOC inside the battery model. Then, with an adaptive method, it compares the measured cell terminal voltage with the model prediction output. Finally, the two values are compared and the computed relative error is used to correct the internal state of the cell model.

### 2.3.1 Coulomb counting method

The most used model is the Coulomb counting method (or Ampere-hour counting method), for its straightforward implementation and relatively good results. However, it is accompanied by an increasing error, due to measurements uncertainty and non-constant capacity values. The *Coulomb counting method* considers the SOC as the ratio between the available charge and the nominal value. It calculates the remaining capacity simply by integrating the charge transferred in or out of the battery. In order to make this model as accurate as possible, it requires precise measurement of the battery current and accurate estimation of the initial SOC. Starting with a known value of capacity, the battery SOC can be calculated by integrating the charging and

discharging currents over the operating periods through (2.5):

$$SOC = \frac{1}{3600 \cdot Q_{nom}} \int_{\Delta t} i(t) dt \quad (2.5)$$

in which  $Q_{nom}$  is the nominal capacity which represents the maximum achievable capacity [Ah],  $\Delta t$  is the operating period [s],  $i(t)$  is the charging/discharging current with the relative sign [A], 3600 is the conversion factor for the capacity [s/h].

The main issue comes from the fact that, during charging/discharging cycles, there is always a part of charge that is stored inside the cells and cannot be released. That is to say that there are losses during charging and discharging cycles, all of which we should take into account for a more precise SOC estimation. These losses, in addition with the self-discharging process, are going to generate an accumulating error. Furthermore, there is always a measurement noise which comes from non-ideal instruments. Obviously, the accuracy of the SOC estimation method is affected by discharging and charging efficiencies under different ambient temperature [25]. Once again, as well as for other parameters, one can often neglect the temperature dependency of our model.

To include (2.5) in the final state-space model we will use later, it is convenient to express the SOC with its differential form:

$$\dot{SOC}(t) = \frac{1}{3600Q_{nom}} i(t) \quad (2.6)$$

## Chapter 3

# Methodology

### 3.1 Implemented battery model

#### 3.1.1 Preface and observations

The model implemented in this thesis, is a modification of the classical TTC model discussed in Section 2.2.1. The already modified electric circuit, is integrated with an adaptive method, the Kalman Filter technique, which is able to continuously estimate the internal state by using measurements updates. The filtering working principle is illustrated in next section. Such a technique is adopted to have a more precise battery state estimation, by comparing at every time the computed model output with the actual measurement. Applying this tool at the cell level means that, given a certain time  $t$ , one estimates the internal state  $x(t + 1)$  for the considered cell at the next time step  $(t + 1)$  and then, comparing the model prediction with the measurements, is possible to give a "weight" to the model output. In other words, when the model response is close to the new measurement, the estimate is trusted more. If the model output is very different from the actual state, for the next assessment, the last measured state is trusted more.

During our model procedure, measurements have been taken at relatively high resolution, with whom, the classical TTC model was not capable to represent all the internal dynamics of the battery. Therefore, the model has been improved by adding a third branch, accounting for the fastest electrochemical dynamics, and a controlled voltage source  $E$  (the equivalent electric circuit is shown later in Fig. 3.1). As the previous two branches, the third one is a parallel connection between a resistor  $R_3$  and a capacitor  $C_3$ . The voltage source  $E$  shows its dependency on the SOC, and one can derive a linear function between the two items, as expressed in (3.19). All the other parameters are exactly the same of the TTC model. In effect, the additional state of the third order model represents the "fast dynamics" and they cannot be observed having measurements at low resolution. Going at larger time intervals, two time constants are enough to capture all the dynamics which come from the device internal structure. In this application, all the measurements are refreshed with a time interval of 1 second as explained in Section 4.2, therefore, the three branches model will be more accurate.

### 3.1.2 Kalman-filter origins and definition

Kalman filtering is a widely used recursive procedure to optimize the estimation of the internal state of a dynamic system, accounting for measurements noise and model uncertainty of the system [27]. A filter is by definition a device capable to remove or attenuate unwanted items [28]. In our application the «*filter*» is a mean responsible of forming good estimate from noisy data. This technique is based on a much older theory, the least-squares estimation introduced by Gauss in 1795. It arises in the astronomical field, in which the studies of heavenly bodies motion was done starting from measurements data. Defined a set of equations containing some parameters to describe the problem, it was necessary to find the value of those parameters. In order to estimate them, Gauss found out that there was a minimum required number of observations. He introduced the "minimization of the residuals" concept: the difference between the observed values and the predicted estimates has to be as small as possible. It defines the problem in a probabilistic way, stating that errors are unpredictable and uncontrollable. In this sense, the most suitable value of the unknown parameters is the most probable one, namely the one in which the sum of the squares of the residual multiplied by the precision is minimum. In a certain way he anticipated the "maximum likelihood method" concept, which was introduced by Fisher later on. Years later, Kolmogorov and Wiener developed a "linear minimum mean-square estimation" technique which gives the foundation for the development of the Kalman filter theory. [29]

The main advantage of the Kalman-filter with respect to the other filtering techniques, is the fact that each update estimate of the state is computed only from the previous estimate and the new input data. So, in contrast to other techniques, one needs to store only the previous estimate, eliminating the need of storing the entire previous observed data, by making it easier to run in real time. Kalman filter is a two steps process: "predict" and "update" phase. The *prediction* phase produces estimates of the current state variables, along with their uncertainties. These estimates are known as a priori state estimates, because it does not include observation information from the current timestep. Once the outcome of the next (noisy) measurement is observed, these estimates are updated using a weighted average of the system's predicted state and of the new measurement, with more weight being given to estimates with higher certainty. This constitutes the *update* stage, and its purpose is to improve the estimate in a way that values with smaller estimated uncertainty are "trusted" more. The weights are calculated from the covariance, a measure of the estimated uncertainty of the prediction of the system's state. The result is a new, more accurate, estimate. The algorithm is recursive, thus this process is repeated at every time step. The filter response can be seen in terms of the Kalman filter gain, which represents the relative weight given to measurements and state estimate. It can be tuned as function of the particular performance one wants to achieve: "high gain" means the measurements are trusted more, "low gain" indicates the model output is more reliable. Another advantage is that, in most applications, the internal state is not fully measurable (or not at all) and, it is estimated by combining a series of measurements, and the Kalman filter can be used to correct those estimates [30].

The transition from the real system to the model, including Kalman Filtering technique, is explained in [31] and summarized below. First of all, it is important to highlight the following

concepts:

- *Real process* - is the real system process, producing signals detected by sensors.
- *State-space mathematical model* - is a way to predict the future behavior of the real process, but it does not exist physically. It consists in a set of first order differential equations, to describe the system dynamics. It has some stochastic inputs, accounting for the randomness of the real process.
- *Kalman Filter* - is a system to be implemented digitally.

It is also important to note that the state variables do not always represent a physical quantity, and, as we will see in the next section (3.1.3), not all of them can be extrapolated by using only physical quantities and actual measurements. What we basically can do, is to use powerful tools able to find the most probable value of those variables. It will be better explained later on.

### Stochastic state-space mathematical models

The state-space mathematical model must be, as said above, a linear system. Both the continuous and discrete form are given below. The continuous form is:

$$\begin{cases} \dot{x}(t) = A_c x(t) + B_c u(t) + H_c d\omega \\ y(t) = C x(t) + D u(t) + G g \end{cases} \quad (3.1)$$

where  $y$  is the model output (observable),  $x \in \mathbb{R}^n$  a system state vector,  $n$  model order,  $A_c$  system matrix,  $B_c$  is the input system matrix,  $H_c$  the input disturbance matrix,  $C$  input measurement matrix,  $D$  feedforward matrix,  $G$  measurement noise matrix,  $g$  is a independent and identically distributed (i.i.d.) standard normal noise,  $u$  input vector,  $\omega$  a  $n$ -dimension standard Wiener process.

The continuous model can be written in the discretized form as:

$$\begin{cases} x(k+1) = A(k)x(k) + B(k)u(k) + H(k)\omega(k) \\ y(k) = C(k)x(k) + D(k)u(k) + G(k)g(k) \end{cases} \quad (3.2)$$

in which  $k$  is the observation time instant, and all the other variables have exactly the same meaning of the continuous form. However, the matrices in the discrete form are not the same as before. They need to be adjusted to the new formulation.

The terms associated to process and measurements noise vectors,  $H$  and  $G$ , are necessary to implement Kalman filtering for state reconstruction. Both the measurement noise  $g(k)$  and the process noise  $\omega(k)$  are assumed to be additive, white and Gaussian, with zero mean.

### Kalman Filter algorithm: Rigorous mathematical formulation

The Kalman Filter to a state-space model must be a deterministic linear system, as it must be easily implemented in, for example, a computer. The equations for the Kalman filter are:

$$\begin{cases} \hat{x}(k+1|k+1) = A(k)\hat{x}(k|k) + B(k)u(k|k) + K(k)v(k|k) \\ \hat{y}(k|k) = C(k)\hat{x}(k|k) + D(k)u(k|k) \end{cases} \quad (3.3)$$

The symbol (  $\hat{\phantom{x}}$  ) highlights the fact that the considered terms are estimates, to make clear that the internal state is not measurable. However, it requires to know the internal state vector initial condition  $\hat{x}(0|0)$ :

$$\hat{x}(0|0) = x_0 \quad (3.4)$$

In (3.3),  $\hat{x}(k+1|k+1)$  is the estimate for the next time step,  $\hat{x}(k|k)$  represents the updated current state-estimate based on the information collected up to instant  $k$ ,  $\hat{y}(k|k)$  is the current estimate of the model output,  $y(k)$  is the current real process output and the matrix  $K(k)$ , is known as the Kalman open-loop gain. The term  $v$  is wide-sense white-noise process, representing the difference between the actual measurement  $y(k)$  and the predicted model output  $\hat{y}(k|k)$ . Its expression is given in the following equations:

$$v(k|k) = y(k) - \hat{y}(k|k) \quad (3.5)$$

$$v(k|k) = y(k) - [C\hat{x}(k|k) + Du(k|k)] \quad (3.6)$$

The Kalman gain matrix  $K(k)$  is given by the following formula [32]:

$$K(k) = [A(k)P(k)C(k)^T + H(k)G(k)^T][C(k)P(k)C(k)^T + G(k)G(k)^T]^{-1} \quad (3.7)$$

where  $P$  is the estimates' error covariance matrix:

$$P(k) = E[(x(k) - \hat{x}(k+1|k+1))(x(k) - \hat{x}(k+1|k+1))^T] \quad (3.8)$$

$E$  is the expectation operator and it can be calculated by the *Riccati difference equation* in (3.9), imposing the initial value  $P(0)$ :

$$P(k+1|k+1) = A(k)P(k|k)A(k)^T + H(k)H(k)^T - [A(k)P(k|k)C(k)^T + H(k)G(k)^T][C(k)P(k|k)C(k)^T + G(k)G(k)^T]^{-1}[A(k)P(k|k)C(k)^T + H(k)G(k)^T]^T \quad (3.9)$$

$$P(0) = P_0 \quad (3.10)$$

Therefore, to implement the Kalman filter, the process covariance matrix  $P(k)$  is computed from the Riccati equation in (3.9) and the gain matrix  $K(k)$  from (3.7). Assuming that the matrices  $A, B, C, D, H$  and the initial conditions for the state vector and covariance matrix,  $x_0$  and  $P_0$ , are known, all these calculations can be done offline, before starting the observations. Since these coefficients are precomputed, the relative computational effort is minimum.

## Kalman Filter implemented algorithm

The Kalman filtering technique usually implemented in electrical engineering applications, in literature, presents simplified equations (see for example [33], [34], [35], [36], [37]). The formulation is given without going too much in detail with the mathematical derivations. For the following considerations, we assume the matrices  $A, B, C, D, H, G$ , as well as  $P$  and  $x$  initial conditions, known and constant. The purpose is to use the new measurement  $y(k)$  to update the a priori estimate  $\hat{x}(k|k)$  of the unknown state  $x(k)$ . It allows to express the a posteriori estimate  $\hat{x}(k+1|k+1)$  as a combination of the previous estimate and the new measurement, relying on the Kalman gain  $K$ , which has to be determined, and the *innovation* process  $v(k)$ , representing a measure of the information contained in  $y(k)$ . The Kalman Gain  $K$  is defined as a function of the a priori covariance matrix as expressed in (3.16). We can summarize as follows:

### 1) Prediction step

$$\text{State expected value} \quad \hat{x}(k+1|k) = A(k)\hat{x}(k|k) + Bu(k|k) \quad (3.11)$$

$$\text{Measurement prediction} \quad \hat{y}(k|k) = C\hat{x}(k|k) + Du(k|k) \quad (3.12)$$

$$\text{Expected covariance matrix} \quad P(k+1|k) = AP(k|k)A^T + HH^T \quad (3.13)$$

$$\text{Innovations process} \quad v(k) = y(k|k) - \hat{y}(k|k) \quad (3.14)$$

### 2) Update step

$$\text{Updated internal state} \quad \hat{x}(k+1|k+1) = \hat{x}(k+1|k) + Kv(k) \quad (3.15)$$

$$\text{Updated Kalman Gain} \quad K = P(k+1|k)C^T[CP(k+1|k)C^T + GG^T]^{-1} \quad (3.16)$$

$$\text{Updated covariance matrix} \quad P(k+1|k+1) = [I - KC]P(k+1|k) \quad (3.17)$$

The algorithm from Eq. (3.11) to (3.17) described in this section, is the one will be implemented to adapt our battery model to real-time measurements.

### 3.1.3 Kalman filter technique - based model considering three time constants and variable voltage source

The relative equivalent electric circuit of the Three Time Constants model is represented in Fig. 3.1 and follows the state-space model formulation in (3.18). The battery voltage model is formulated by using the continuous time stochastic state-space model representation as presented in [38]:

$$\begin{cases} dx = A_c x(t)dt + B_c u(t)dt + H_c d\omega \\ v(t) = C x(t) + D u(t) + G g \end{cases} \quad (3.18)$$

where  $v$  is the model output and battery cell terminal voltage,  $x$  a system state vector,  $A_c$  system matrix,  $B_c$  is the input system matrix,  $H_c$  the input disturbance matrix,  $C$  input measurement matrix,  $D$  feedforward matrix,  $G$  measurement noise matrix,  $g$  i.i.d. (independent and identically distributed) standard normal noise,  $u$  input vector,  $\omega$  a standard Wiener process. The

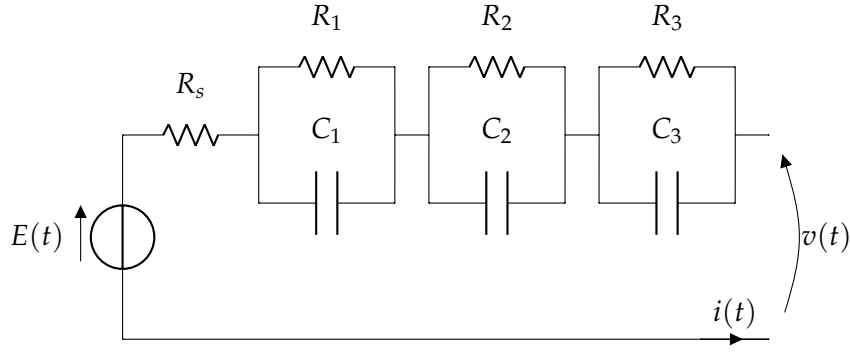


**Fig. 3.1.** Augumented TTC model containing three time constants and SOC dependent voltage source

terms associated to process and measurements noise vectors,  $H_c$  and  $G$ , are necessary to implement Kalman filtering for state reconstruction.

The parameters constituting the electric circuit in Fig. 3.1 can be described as follows. In a nutshell,  $R_s$  is the battery series resistance representing the energy losses during charge or discharge cycles,  $C_3, R_3$  are the resistance and the capacitance accounting for the fastest electric dynamics,  $C_2, R_2$  are the resistance and the capacitance accounting for the delayed electric dynamics,  $C_1, R_1$  are respectively the capacitance and the resistance of the first branch, modeling the slowest electrochemical dynamics,  $E$  is the cell open circuit voltage. Their meaning, from the electrochemical point of view, is accurately discussed in Section 2.2.1.

*a) Open circuit voltage dependency on the SOC*

The controlled voltage source  $E$  (it is sometimes indicated as  $V_{oc}$ ), which represents the open circuit voltage of the battery, depends on the battery SOC as well. It can be experimentally evaluated that the open circuit voltage  $E$  increases linearly with the SOC. Even if we consider small SOC intervals, the variations of the open circuit voltage inside each range is still present. Not considering its dependency on the SOC would give large errors. Therefore, it is represented as a linear function of the battery SOC [38], as shown in (3.19):

$$E(SOC(t)) = \alpha + \beta \cdot SOC(t) \quad (3.19)$$

where  $\alpha$  and  $\beta$  are non-dimensional parameters to identify.

Actually, going at very low or very high SOC, this assumption is not accurate anymore. The closer we get to the upper and lower limits, the more accentuate the nonlinearity is. Since the function in these two zones is very tricky to represent, we assume the linear function can be valid for all the possible battery states. In Fig. 3.2 there is the curve derived from experimental data. It is clear that it is good approximated by a linear function (the residual is roughly 0). Unfortunately, in the area where we expect non linear dynamics, is very difficult to have useful information because of the currently security systems. In fact, as soon as we get closer to the limits, if the value of power is too high, the BMS makes that the contactors connecting the battery to the converter (it converts battery DC power to AC to exchange with the grid) are

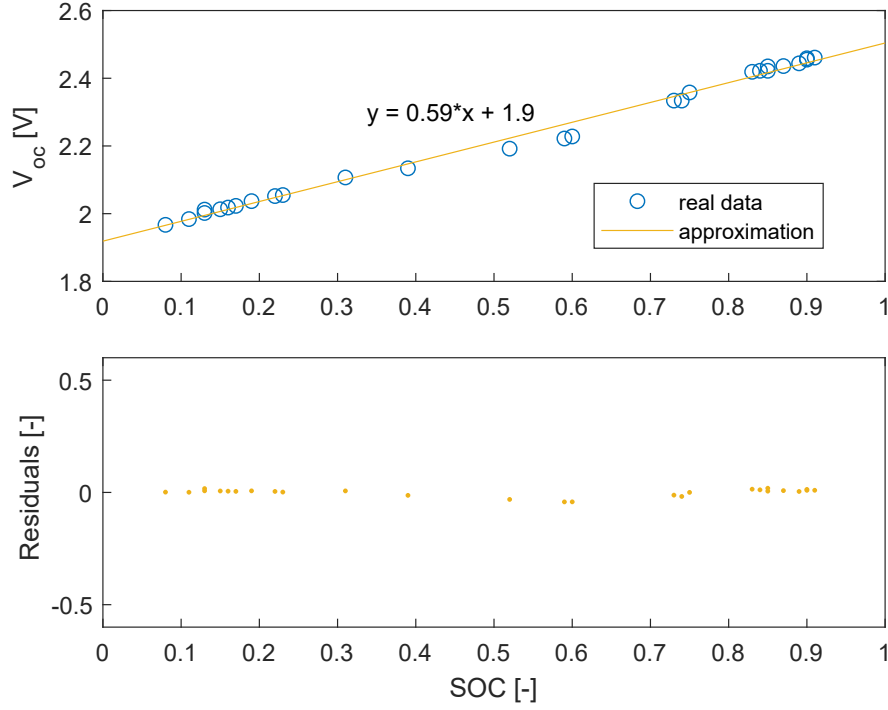


**Fig. 3.2.** Above: Open Circuit Voltage - State Of Charge linearity for a generic battery cell. Below: Fitting residuals.

immediately disconnected. It causes an abrupt cessation of the normal function of battery and converter, making that the needed data cannot be collected. Moreover, it requires a manual restart of both devices.

*b) Series resistance*

The series resistance  $R_s$  represents the electrochemical losses during charging and discharging cycles. As already mentioned, it can be interpreted as a voltage drop across the circuit. It has a precise physical meaning and it can, therefore, be calculated. It is empirically calculated by following (3.20):

$$R_s = \left| \frac{\Delta V}{\Delta I} \right| \quad (3.20)$$

where  $\Delta V$  is the instantaneous voltage variation occurring in correspondence to a large step in the input current  $\Delta I$ .

The model is given by applying Kirchhoff laws to the circuit in Fig. 3.1 and then, linearizing it approximating the exponential term with its Taylor series. The matrices for describing the state-space model, assuming a continuous system, are illustrated in (3.21).

$$x(t) = [v_{C_1}(t) \quad v_{C_2}(t) \quad v_{C_3}(t) \quad SOC(t)] \quad u(t) = [i(t) \quad 1]^T$$

$$\begin{aligned}
A_c &= \begin{bmatrix} -\frac{1}{R_1 C_1} & 0 & 0 & 0 \\ 0 & -\frac{1}{R_2 C_2} & 0 & 0 \\ 0 & 0 & -\frac{1}{R_3 C_3} & 0 \\ 0 & 0 & 0 & 0 \end{bmatrix} & B_c &= \begin{bmatrix} \frac{1}{C_1} & 0 \\ \frac{1}{C_2} & 0 \\ \frac{1}{C_3} & 0 \\ \frac{1}{Q} & 0 \end{bmatrix} & C &= [1 \quad 1 \quad 1 \quad \beta] & D &= [R_s \quad \alpha] \\
& & & & & & & (3.21) \\
& & & & & & & K_c = \text{diag}(k_1, k_2, k_3, k_4) \quad G = \sigma_g^2
\end{aligned}$$

Where  $v_{C_1}, v_{C_2}, v_{C_3}$  are the voltage drops across the three RC branches, SOC in the state of charge value. The  $i$  is the current, which it is considered positive during charging and negative during discharging for the adopted model convention.  $R_s, R_1, C_1, R_2, C_2, R_3, C_3, \alpha, \beta, k_1, k_2, k_3, k_4, \sigma_g$  is the set of parameters constituting the model which need to be estimated. They change according to SOC,  $C_{\text{rate}}$  and temperature, as a consequence of the nonlinear phenomena described in Section 2.1.1. The series resistance  $R_s$  and the open circuit voltage  $E$ , can be computed with the equations (3.19) and (3.20), while all the other parameters require a dedicated parameters identification from stored measurements. This process is described in the following section.

### Parameter identification

An accurate parameter estimation is essential to have a good prediction model. For some simplified models, it is possible to compute the different parameters by doing ad hoc measurements, but they require particular instruments and are very time spending. The estimation is more often based on tools such as maximum likelihood and a posteriori estimation, which use training data as resources. They allow to estimate all the items at the same time, with the same set of measurements. When using grey-box models, there is the advantage to have some physical knowledge or other kind of prior informations which can be included directly in this step. The accidental process and measurement noise do not affect the parameter estimation, since they are accounted for in the process and measurement noise terms. Therefore they are estimated simultaneously with all the other model parameters. They quantify the uncertainty of the model, giving an assessment on the quality of the model. [39, 40] To our purpose, all these studies have not been investigated in detail, though the data have been processed into a Matlab script (ParameterIdentification.mat) and then the parameters estimated with the *greyest* function.

### The Pseudo Random Binary Signal

The choice of the right input signals is also very important. In order to build a system which contains all the different dynamics, we would like to have a white noise signal because it excites all the frequency modes in the system. White noise is a random signal with a flat power spectral density. The signal contains equal power within a fixed bandwidth at any center frequency. By having power at all frequencies, the total power of such a signal is infinite [41]. Since the white noise cannot be physically realized, the Pseudo Random Binary Signal is a good alternative for linear model identification. PRBS is a signal which has similar characteristics to the white noise. It is a rectangular signal of various width and it can assume only two values which change pseudo-randomly at multiples of the sampling time and it repeats several times [42].

Such a signal which gives a useful stimulus for this kind of analysis, can be generated digitally, using only one instrument. It can be given alone or in addition to the usual working signal. The output response is measured and postprocessed in order to have all the necessary information [43]. In our case the PRBS signal is implemented in LabVIEW, and given in terms of power. Each experimental session lasts for 1 hour and clocked at 1 minute. More details are presented in Chapter 4.

## 3.2 Computation of the maximum power flexibility of the fully battery stack based on the cell-level model

### 3.2.1 Cell inconsistency problem

A battery is made of a certain number of cells (780 cells in our case), for increasing the available power and energy the user needs to supply. In order to improve battery abilities, several parallel and series connection are required. More in detail, parallel connections increase the total capacity, whereas series connections give a higher output voltage. Typically, any on board BMS is able to monitor each cell voltage in order to avoid overcharge or overdischarge might occur. Analyzing these data, it is possible to see that not all the cells have the same behaviour. By subjecting cells in the same battery pack to the same current, due to non-ideal internal electrochemical dynamics, they reach different values of terminal voltage. By referring to the battery used for the experiments, the available current value is the global current. In effect, during normal operations, every user does not really care about the cell current, because batteries input and output are overall defined. In addition, typically current value is not available for single cells. Indeed, if on one hand the voltage can be measured at the cell level, on the other hand the cell current is not measurable. In fact, it is hard to measure the current of each cell because it would require additional current sensors, which are expensive and difficult to install [44].

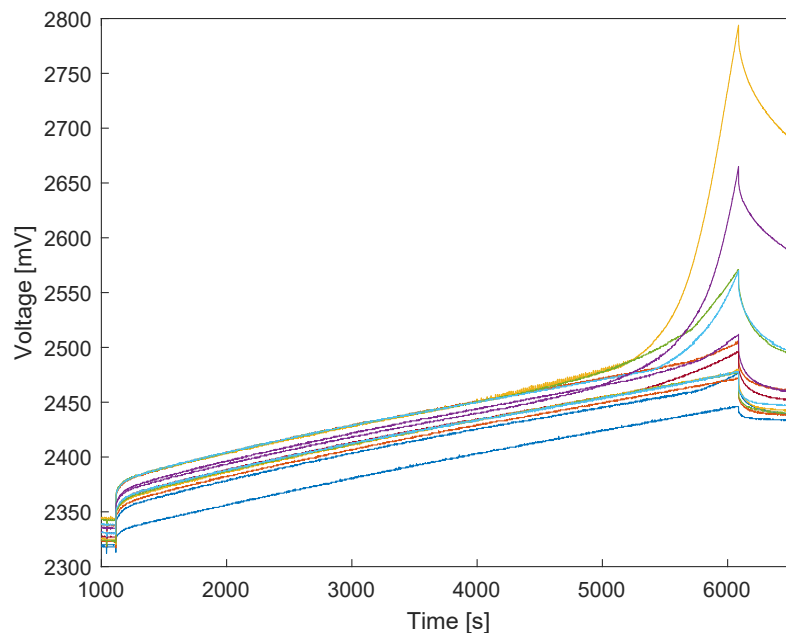


Fig. 3.3. Cell voltage per module in the same battery pack

Figure 3.3 shows some data relative to the 25 kW/ 25 kWh battery pack that will be used for the experiments. The related BMS is monitoring the most and least charged cell for each module. In the graph, since measurements have been taken while charging, the highest voltage per module has been plotted, which is more interesting since it has the most critical value. The fact that one of the cells is out of the target range (greater than 2700 mV) was not visible looking

at the global rack. It is also possible to notice that there are some interceptions between different curves: the most critical cell is not always the same one.

In general, the more numbers of the cells connected in battery systems, the greater of the difference exist in cells parameters [45]. The cell inconsistency problem may reduce the battery performance, as well as operating efficiency. Once many cells are assembled into a battery pack, the performance of the battery pack cannot be evaluated simply considering all the cells together. The worst cell, namely the one with the highest and the one with the lowest voltage, to determine the whole battery pack performance. Nevertheless, the same considerations are still valid in terms of current. Even if this is not available, one can estimate that value at the cell level, for ensuring the best achievable operating conditions of the device. The cell inconsistency problem can be caused by multiple factors, such as manufacturing process, impure materials, errors during operations, different degradation rate due to different temperatures or currents, etc [24]. The current state of art does not allow to remove completely the problem, but running the battery in the right way helps to slow down and delay that phenomenon. The whole rack operations have to be limited by looking at the "worst" cell in the pack. Some cell-balancing techniques have been also proposed for optimizing the battery performances. A review is given in [46]. According to it, one can distinguish passive and active balancing methods:

1. Passive methods implementation is very simple, being based just on temperature increment by overcharging the battery. However, such methods are not effective on a big number of cells and they cannot be used for Lithium ion batteries because this kind of batteries does not support overcharging without going through permanent cells damage.
2. Active balancing methods rely on the use of external circuits to equally distribute the energy among cells. This is the only applicable method for Lithium based batteries since they must to be kept in the working temperature range. They can be grouped in three categories: shunting method, shuttling method and energy converter method. They consist in the addition of electrical components, such as switches, resistors, transistors, inductors, etc.

Even if many methods have been proposed, they have limited effectiveness and huge costs, finding rare actual applications. Therefore, good battery control is essential.

### **3.2.2 Formal computation of the battery cell active power constraint**

Battery set points are usually given in terms of power. The simplest way to accurately control it, is to impose the battery flexibility as power function, by ensuring that all the safety limits are respected. Namely, the most critical cell is in the allowed operating range in terms of current and voltage at each moment. In this sense, we should be able to impose the conditions at time  $t$  such that at the next time instant,  $t + \Delta t$ , we are sure that all the limits are still respected. In order to compute the battery cell operative bounds in terms of active power for the next time step, the procedure illustrated for the rack in [47] and [48] is followed. In the mentioned work the implemented battery model is the classical TTC model. Therefore, some modifications are

required. It should be noted that, for the reasons explained in Section 3.2.1, the cell inconsistency problem has to be accounted for. Hence, power constraints have to be determined at the cell level, and then translated to the global rack by using the method indicated in Section 3.2.3.

The power of the battery cell is given by (3.22):

$$P(t) = v(t) \cdot i(t) \quad (3.22)$$

The way we defined the model, a positive value of the  $P(t)$  is associated to the charging mode and a negative value to the discharging. In this sense, the maximum power  $P_{max}$  represents the charging and the minimum  $P_{min}$  the discharging power. At time  $t$ , a set of all the feasible active power set points at the next time step are computed, accounting for the limits imposed by the cell characteristics, in terms of voltage and current:  $V_{min}, V_{max}, I_{min}, I_{max}$ .

#### 1) Voltage constraints

To find the limit the voltage bounds impose on the maximum and minimum power, we should represent the power as a function of the voltage itself. The following steps aim towards this goal.

From (3.22) we can derive (3.23):

$$i(t) = \frac{P(t)}{v(t)} \quad (3.23)$$

In the following equations, for simplifying the reading, the time dependency has been omitted, but it is worth noting that we are still considering the active power with its time dependency.

Using (3.23) and (3.21) in (3.18) and neglecting the measurement noise  $G$  and the process noise  $H$ , one can write:

$$v = Cx + Du \quad (3.24)$$

$$v = Cx + R_s i + \alpha \quad (3.25)$$

$$v = Cx + \frac{R_s P}{v} + \alpha \quad (3.26)$$

$$v^2 - (Cx + \alpha)v - R_s P = 0 \quad (3.27)$$

$$v^2 - C_\alpha v - R_s P = 0 \quad (3.28)$$

Solving (3.28) we get the  $v(t)$  as a function of  $P(t)$  at a given time  $t$ :

$$v(t) = \frac{C_\alpha \pm \sqrt{C_\alpha^2 + 4R_s P}}{2} \quad (3.29)$$

To see which is the correct solution, we have to distinguish two cases.

- Charging phase: Since we assumed that the power flow is positive during charging and the voltage is always positive, the only feasible solution is the one linked to the positive sign.
- Discharging phase: The corresponding power flow is negative, so that both the solutions

linked to the positive or negative sign give positive voltage value and they might therefore be acceptable. However, we have to take into account the fact that the voltage has a continuous behaviour. In order to have this continuity also on the zero-crossing of the power flow (going from charge to discharge and vice versa), the only valid solution is the one related to the positive sign, as well as for the charging case.

From the square root term in (3.29), one can compute the critical power  $P_{cr}(t)$ . The operational power has to be always greater than or equal to the critical value in (3.30).

$$P_{cr}(t) = -\frac{C_\alpha^2}{4R_s} \quad (3.30)$$

By rewriting (3.29), we can finally obtain  $P(t)$  as a function of  $v(t)$ , as it is shown in (3.31) and in its plot in Fig. 3.4:

$$P_{dc}(t) = \left(\frac{1}{R_s}\right)v(t)^2 - \left(\frac{C_\alpha}{R_s}\right)v(t) \quad (3.31)$$

$$P(t) = f(v(t)) \quad (3.32)$$

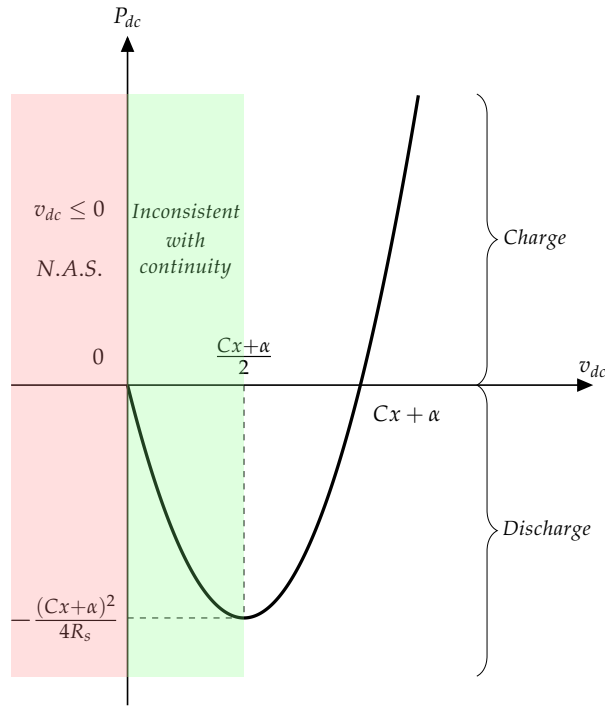


**Fig. 3.4.** Active power as a function of active voltage

The red area corresponds to negative values of voltage, hence, by intrinsic definition of voltage, it is not acceptable. Likewise, the solution linked to the green area is inconsistent with continuity. It would indicate an increase of voltage increasing the discharging power, which is physically infeasible. Since the voltage increases with the voltage in a monotonic way (see [48] for proof), the maximum power  $P_{max,v}(t)$  is reached only during charging phase, when the voltage is equal to the maximum voltage  $V_{max}$ . On the contrary, the minimum power is reached only during discharging, since the voltage decreases during this phase. The minimum power

$P_{min,v}(t)$  is the one related to the minimum cell voltage  $V_{min}$ . On the other hand, the minimum power must respect the continuity requirement. For that purpose, we cannot accept as limiting power a value that comes from voltage lower than the critical value  $v_{cr}$ , whose expression is given in (3.33):

$$v_{cr} = \frac{Cx + \alpha}{2} \quad (3.33)$$

Moreover, the critical voltage is the value of voltage that gives the critical power  $P_{cr}$  in (3.30). It is worth noting that  $P_{cr}(t)$  is not for nothing the power corresponding to the function minima.

In the end, the power constraints imposed by voltage limits are computed by (3.34):

$$\begin{cases} P_{max,v}(t) = f(V_{max}) \\ P_{min,v}(t) = f(\max(V_{min}, (\frac{Cx+\alpha}{2}))) \end{cases} \quad (3.34)$$

## 2) Current constraints

In order to find the power limits imposed by the current, as well as we did for the voltage, it is necessary to find a relation between the active power  $P(t)$  and the active current  $i(t)$ . From (3.18) and (3.22), neglecting the measurement noise, one gets:

$$v = Cx + Du \quad (3.35)$$

$$\frac{P}{i} = Cx + R_s i + \alpha \quad (3.36)$$

From which we can write the power  $P(t)$  as a function of the current  $i(t)$ , as expressed in (3.37) and (3.38):

$$P(t) = R_s i(t)^2 + (Cx + \alpha) i(t) \quad (3.37)$$

$$P(t) = g(i(t)) \quad (3.38)$$

The function  $P_{dc}(t) = g(i_{dc}(t))$  expressed in (3.37) is plotted in Fig. 3.5. Regarding the charge, the power increases again increasing the current. Consequently, the maximum power  $P_{max,i}(t)$  is limited by the maximum acceptable current  $I_{max}$ . Concerning the discharge mode, instead, the power decreases going at lower current value. Therefore, the minimum power  $P_{min,i}$  is the one corresponding to the minimum cell current  $I_{min}$ . Obviously, we have to respect the continuity problem here too. It means that all the voltages included in the blue area are infeasible. For that reason we have to add one more constraints, namely the value of the power given from the critical voltage  $v_{cr}$ , given in (3.39):

$$v_{cr} = -\frac{Cx + \alpha}{2R_s} \quad (3.39)$$

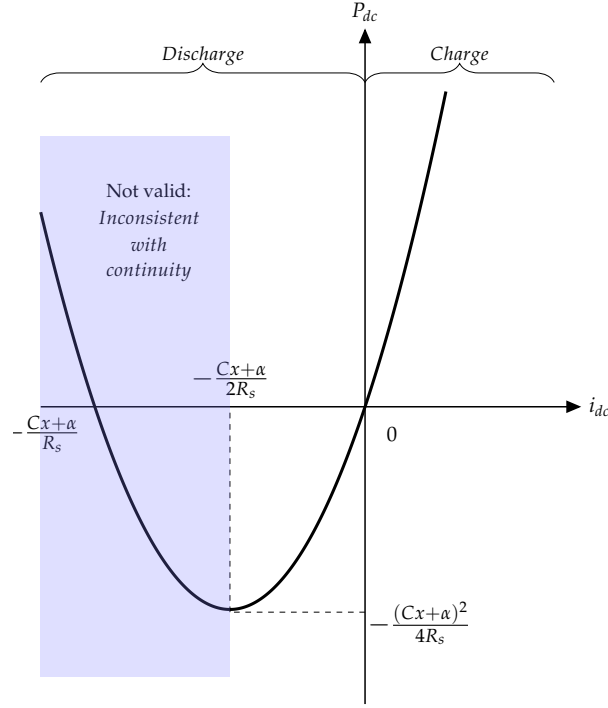


Fig. 3.5. Active power as a function of active current

Combining all the current requirements and the continuity consistency, the current constraint is summarized in (3.40):

$$\begin{cases} P_{max,i}(t) = g(i_{max}) \\ P_{min,i}(t) = \max(g(i_{min}), g(-\frac{Cx+\alpha}{2R_s})) \end{cases} \quad (3.40)$$

Once we have the value of the power limited by the current or voltage, at each time we have to take the more limiting one between the two. In other words, the absolute maximum power  $P_{max}$  is the more restrictive one between  $P_{max,v}$  limited by the voltage and  $P_{max,i}$  limited by the current. In the same way, the absolute minimum power  $P_{min}$  is the more restrictive one between  $P_{min,v}$  limited by the voltage and  $P_{min,i}$  limited by the current. For the sake of simplicity, this is summarized in (3.41):

$$\begin{cases} P_{max} = \min(P_{max,v}, P_{max,i}) \\ P_{min} = \max(P_{min,v}, P_{min,i}) \end{cases} \quad (3.41)$$

### 3.2.3 Maximum power flexibility computation

As is evident from this study, the maximum power flexibility of a battery cannot be done without using a reliable model. In effect, it is based on analytical functions  $f$  and  $g$  to link the power to the limiting values of current and voltage, whose depend also on model parameters. Once the model is completely defined, the maximum power flexibility is calculated at the cell with (3.41). First of all, we have to recall that the maximum power flexibility computation has to be performed at cell level. Then, knowing the values of the power  $P_{max/min}$  and the cell

voltage  $v$ , is possible to compute the corresponding current (at cell level) by using (3.42):

$$i_{max/min} = \frac{P_{max/min}}{v} \quad (3.42)$$

With the value of  $i_{max/min}$  is possible to compute the corresponding current for the whole rack. At these point we need an assumption to correlate the cell current to the global current: we can think that the current is equally distributed among the number of parallel connections of the cells,  $N_p$ . Therefore, one can write:

$$i_{rack,max} = N_p \cdot i_{max} \quad i_{rack,min} = N_p \cdot i_{min} \quad (3.43)$$

At this point, the maximum power flexibility for the total stack  $P_{rack,max/min}$ , is derived just by multiplying the gobal current  $i_{rack,max/min}$  by the measured global voltage  $v_{rack}$ :

$$P_{rack,max} = v_{rack} \cdot i_{max} \quad (3.44)$$

$$P_{rack,min} = v_{rack} \cdot i_{min} \quad (3.45)$$

This process is summarized in the flow chart in Fig. 3.6, in which current, voltage and power values can be referred either to the most or least charged cell.

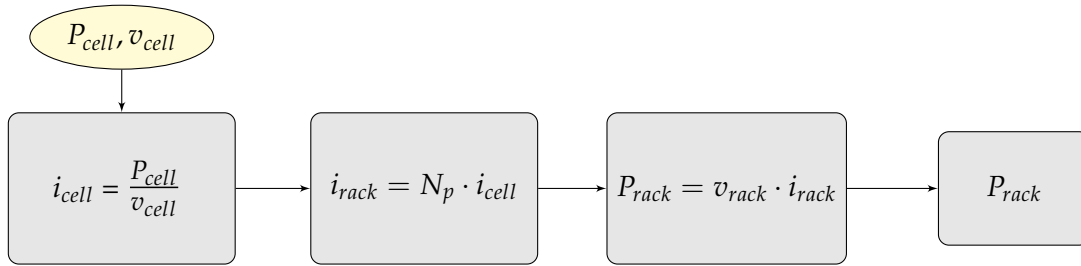


**Fig. 3.6.** From cell to total rack power flexibility: Flow chart

## Chapter 4

# Implementation and Results

### 4.1 Experimental setup



**(a)** 25 kW / 25 kWh Lithium-Titanate battery: The 13 modules can be clearly distinguished and easily accessible.



**(b)** In the front there is the converter, directly connected to the battery. The CompactRIO is on the converter box.

**Fig. 4.1.** Experimental setup: Battery, Converter and CompactRIO

The battery is part of the EPFL low voltage Microgrid, constituted within the Distributed Electrical System Laboratory (DESL). The electricity is mainly produced by photovoltaic panels (peak power 50 kW) and directly used to feed the grid, or it can be stored by batteries (long term) and supercapacitors (short term storage). The battery is shown in Fig. 4.1a. It is directly connected to a AC/DC converter (Fig. 4.1b) which communicates with the electrical grid. The communication between the user and the battery is enabled by a Modbus protocol. The Slave Interface allows the customer to control and communicate with the Storage Rack System (SRS) through the Battery Management System (BMS). [49]. The BMS represents the rack controller which centralizes the operating data of all the battery modules. All the measurements from

BMS, Converter, PMU <sup>1</sup>, are enabled through a LabVIEW project running on a CompactRIO system, which is accessible from all the machines available in the Lab. The messages the user sends through the mentioned project, are directly coded and executed by the BMS. On the other hand, it also provides measurements of the main features of the battery at modules level, as well as at cells level. All these quantities, such as voltage, current, power, temperature, are essential to guarantee a safe use of the device. To that purpose, it also delivers data for error diagnostics. Nevertheless, such a protocol has some limitations:

1. All values are updated with a refresh rate of 1 Hz. This means that data cannot be measured with a resolution higher than 1 second. Actually, considering the big amount of data exchanged between the BMS and the user, this timing becomes even longer.
2. It allows just one communication at the same time. For this reason it is connected to one machine (CRIO) which can communicate with all the computers in the lab. Basically, the CompactRIO serves as a link between the BMS and the users' machines. An illustration of this concept is given in Fig. 4.2.



Fig. 4.2. Battery to end user communication

The battery is characterized by nominal power and energy of 25 kW and 25 kWh respectively, and is composed by 13 modules. Each module is made, in turn, of 60 cells, with 20 serial and 3 parallel connections. Technical data relative to the module are shown in Figure 4.3.

Main Module Characteristics (nameplate)	
N°cells/module	60 (3 parallel and 20 serial connections)
Nominal Voltage	46 V
Nominal Current	90 A
Module Capacity	48 Ah
Total Module Energy	2.2 kWh
Weight	88 kg
Dimension (LxWxH)	550 x 483 x 356 mm

Fig. 4.3. Battery Module data sheet

The CompactRIO constitutes the controller of the system, hosting all operational loops in *main.vi*: DC and AC measurements (using the embedded FPGA <sup>2</sup>), CAN <sup>3</sup> communication with

<sup>1</sup>PMU = Phasor Measurement Unit, is a device which measures the electrical waves on an electricity grid using a common time source for synchronization.

<sup>2</sup>FPGA = Field-Programmable Gate Array, is an integrated circuit designed to be configured by a customer or a designer after manufacturing field-programmable gate array, is an integrated circuit designed to be configured by a customer or a designer after manufacturing

<sup>3</sup>CAN = Controller Area Network, is a robust vehicle bus standard designed to allow microcontrollers and devices to communicate with each other in applications without a host computer.

the power converter, MODBUS communication with the BMS, Data logging and the Battery Agent. The main file is accessible from the computer through different VIs available in the same project, organized as follows:

- *monitoring.vi*. It contains all the measurements available from the FPGA, the Converter, and the BMS. It also shows the most relevant data from the graphical point of view, by ensuring that possible dangerous situations are more intuitive to notice. At the same time, from the same window is possible to start the data log. It is shown in Figure 4.4.



Fig. 4.4. Monitoring front panel

- *controller.vi*. This is the part of the project which allows to directly "control" the battery. It is useful to start the battery remotely and the converter, and to connect/disconnect it to/from the grid. In addition, it states if the devices are correctly connected (green lights on), or if not, what the problem is. The input set point is given in terms of active/reactive power, voltage, frequency or current. It is given on the converter side, therefore should be considered that some losses might occur. It should be noted that, since the connection is allowed by Modbus in both directions, the response timing is still equal or higher than 1 second. The controller front panel is shown in 4.5.
- *power limits.vi* This is actually the Virtual Instrument (VI) that will be coded at the end of the project. It focuses on the main goal of this project: computing the short-term power flexibility of the battery, in terms of maximum charge and discharge power. It will be studied in depth later on.

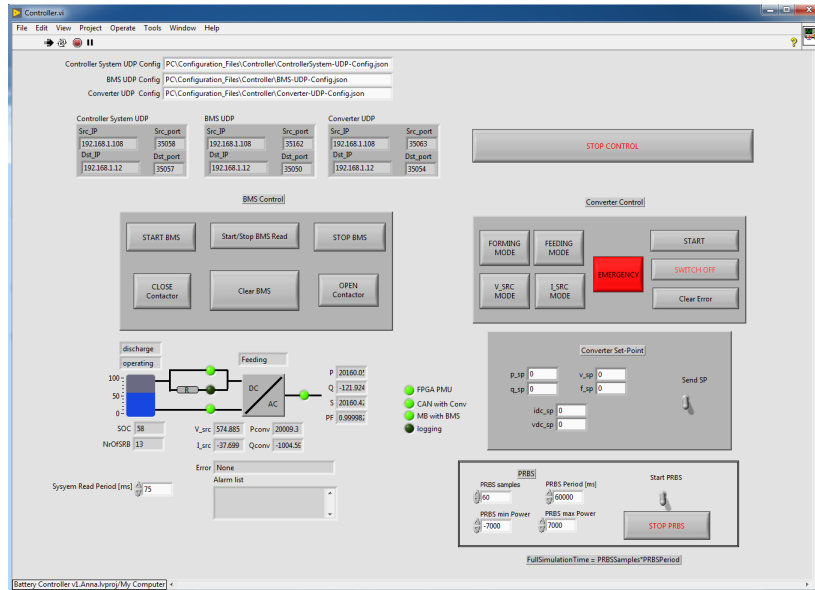


Fig. 4.5. Controller front panel

## 4.2 Definition and implementation of the experiments for the parameter identification

### 4.2.1 Experiment assumptions

As already mentioned, the model parameters depend on three main properties, namely SOC,  $C_{rate}$  and temperature. The dependence between model parameters and both  $C_{rate}$  and temperature is neglected in first approximation. Only their dependence on SOC is considered. Later on, to generalize the model as much as possible, the  $C_{rate}$  dependence has to be considered as well. We will go beyond this obstacle by filtering the model results with the Kalman filter.

Since the model parameters are strongly related to the battery SOC, in order to capture this dependence, a number of PRBS experimental sessions has to be performed when the battery is in different SOC ranges. Ideally, one would like have different set of parameters for each SOC value. However, considering the measurements noise and little time available, 5 experimental sessions have been performed to make it feasible, according to the following SOC ranges: 0-20 %, 20-40%, 40-60%, 60-80%, 80-100%.

The  $C_{rate}$  in particular plays an important role in the modeling procedure. In order to not incur in wrong results, all the experiments have been done with a value of power that is used in normal operations. For the reasons just explained, a PRBS power signal of  $\pm 7$  kW is used. To have a more robust model, the Kalman filter technique takes care of different power/current values.

The temperature variation in this application does not affect the voltage behavior as much as the other features, since the battery is equipped with a temperature control system. One can assume with good approximation that it remains constant during the experiments.

Last but not least, a hypothesis regarding the current measurement is needed as well. It is important to consider that, unfortunately, for any on board battery management system, it is hard to measure the current of each cell in parallel-connected battery packs. This is because it is impractical and expensive to add additional current sensors to a BMS to monitor individual cell current [44]. Only the global current is available. Therefore, we assume in first approximation that the current in each cell is the total current divided by the number of parallel connections, so the third part of the current of the whole battery system:  $I_{cell} = I_{rack}/3$ .

#### 4.2.2 The PRBS signal

As already stated, the PRBS signal is a two levels squarewave, able to excite a wide range of internal electrochemical dynamics, allowing to have plenty of valuable information in a limited amount of time. A first set of parameters have been estimated without taking into account the  $C_{rate}$  influence. Therefore, all the experiments have been done by using the value of the power (active power) used in normal operations. This value has been assumed  $\pm 7$  kW. Such a signal can be directly implemented in LabVIEW, using one of the dedicated Utilities VIs. The relative front panel is shown in Fig. 4.6.

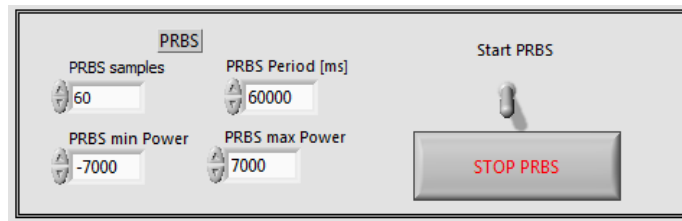


Fig. 4.6. PRBS set point in Controller.vi

The set point values of the PRBS signal can be selected in Controller.vi in terms of power through the controller in the bottom side in Fig. 4.5. During the experimental sessions different set point values have been tested. Several tries have been done in this sense and at the end it has been chosen equal to 1 minute (see Fig. 4.7).

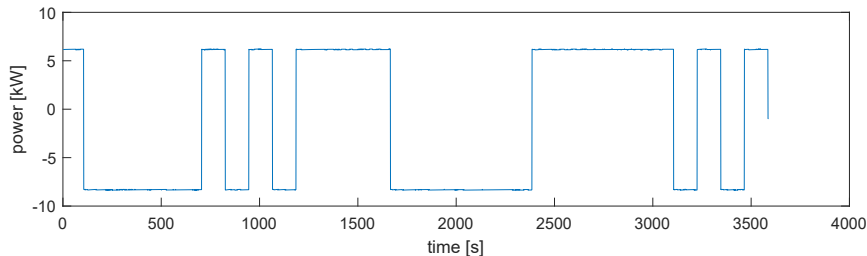


Fig. 4.7. Power PRBS signal

However, going to the upper and lower SOC limits, such a value of power results to be very tricky since it could induce one (or more) of the cell voltages to reach and cross the bounds. Finally, we choose to continue by imposing 60 samples, with a period of 1 minute. Therefore, each experimental session lasts for 1 hour. Simultaneously, all the relevant data are registered

and logged in TDMS files, in particular, the two voltage values (highest and lowest) available for each module, and the total current, which are needed for the identification.

### 4.2.3 Parameter Identification

The parameters identification is the most critical stage, once we have fixed which model we are going to use. As established in Section 3.1.3, for exciting a large number of the battery internal dynamics, a PRBS signal plays an essential role. The intent is to have, for each cell, five different models, with the cell in five different SOC ranges: 0-20%, 20-40%, 40-60%, 60-80%, 80-100% . To perform the experiments we have two main issues:

- Each cell is different from the others, therefore if we perform the experiments looking at the total rack, every cell will be in different SOC ranges.
- At the edges the SOC is not linear with the open circuit voltage. It means that the area where we care more about, is also the most difficult one to study and model.

It is worth noting that the experiments should have been done separately for each cell, given their internal structure and behavioral difference. In fact, considering a wide range of SOC, namely 20 %, we will never find a cell which has exactly the same properties (in terms of SOC and voltage) of another one. Having 13 modules and 20 cells each module, we have 260 mismatched voltages and SOC, as response to the same excitation power.

To have better results, where the  $V_{oc}$ -SOC curve is not linear, we should divide the maximum (80-100%) and minimum (0-20%) SOC ranges into a huge number of smaller intervals in which this characteristic can be assumed linear. In reality, this is difficult to implement in practice, because the more accentuated is the non linearity, the closer we are to the edges and the more difficult is to have significant informations. To make it feasible in terms of time and considering observational errors, we reduce the accuracy by treating few ranges, in which the cells have similiar behavior.

Once all the measurements have been recorded at 1 second resolution for the 26 different available cells, a Matlab script "ParameterIdentification.mat" is created. It uses the *greyest* function to completely identify the model in terms of parameters:

```
idsys = greyest(data, sys, opt);
```

where data, sys and opt are defined as follows:

```
data = iddata(V, u);
sys = idgrey(MDL, param, 'c');
opt = greyestOptions('InitialState', [0;0;0.01*SOC(1)], ...
    'DisturbanceModel', 'estimate', ...
    'Focus', 'prediction', ...
    'SearchMethod', 'auto', ...
    'AutoInitThreshold', true);
```

data is an `iddata` object containing the training data: a time-domain output signal  $V$  (cell voltage) and input signal  $u$  (current). The sample time of the experimental data is 1, thus it is not specified. `sys` is a linear grey-box model with identifiable parameters. `MDL` is the function that relates the model parameters, `param`, to its state-space representation. It is basically expressed in the form of matrices as in (3.21). 'c' indicates that matrices correspond to a continuous-time system. `opt` creates all the options for `greyest`. As initial internal state, we assume all the voltage drops across the three branches are zeros and the SOC is equal to the measured SOC. This assumption can be close to the real value, since all the experiments started after the relaxation phase was almost done. The process and measurement noise matrices ( $H$  and  $G$ ) are both estimated with the model. The error to be minimized during the estimation is the one-step ahead prediction error between measured and predicted output, in order to produce a good predictor model. The numerical search method is set on 'auto', a combination of the line search algorithms. Different methods are used in sequence at each iteration in a way that the computational costs are reduced as much as possible. This procedure is repeated in a loop for all the 26 cells, by ensuring that at the end all the parameters are estimated.

A crucial point was the parameters initialization, required by the `idgrey` function. First of all, we have to notice that, among all the parameters, there are some of them we can directly compute from measurements:  $\alpha, \beta, R_s$ . In this sense, we use the computed values to initialize the parameters, but we keep giving a (very) small degree of freedom, considering possible measurements errors and inaccuracies of the calculation. In effect, even when computing the series resistance, we cannot be totally sure the computed value is the real one, because we noticed some anomalies in the training data. In fact, the voltage drop does not occur instantaneously, but in certain cases it takes more than 1 second. From a macroscopic point of view, we see that the voltage drop is well defined (see Fig. 4.8a), while zooming it in Fig. 4.8b several jumps occur.

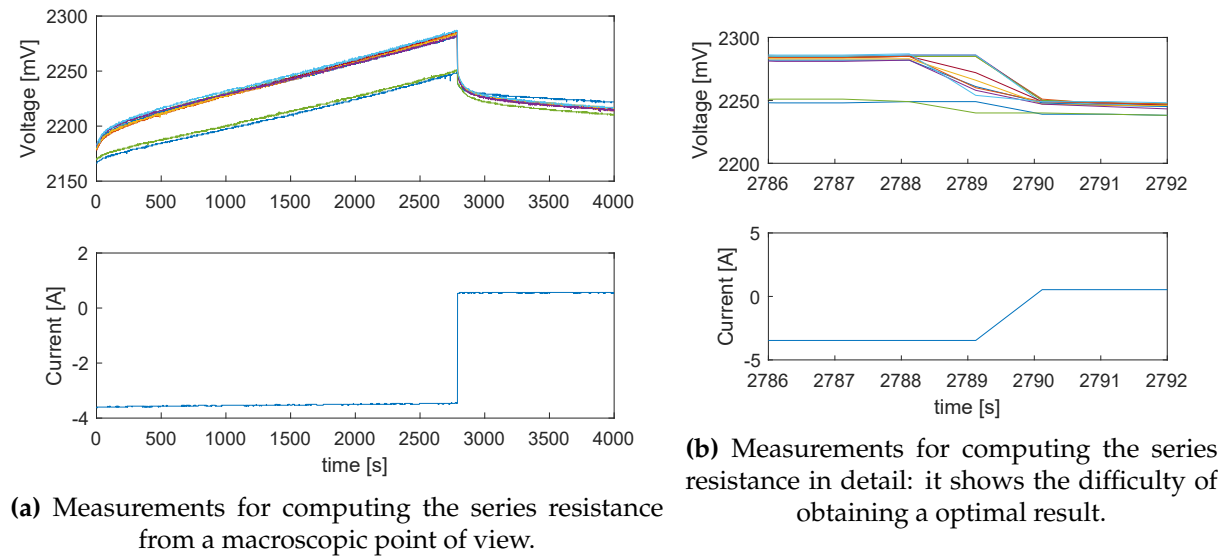


Fig. 4.8. Data for computing the series resistance.

Having measurements at 1 second resolution, it implies that the voltage drop occurs in two

or more steps. This is probably due to delay in data transmission or maybe it is the real behaviour. Anyway, we cannot establish with sufficient certainty which is the cause, hence, it becomes really difficult to have a precise value for the resistance. Moreover, these unexpected values are not consistent in time and SOC. In fact, they change randomly, making that it becomes difficult to account for all the differences given such a big amount of data to process in so little time.

The parameters  $\alpha$  and  $\beta$  are initialized to the value the coefficients assume by approximating the  $SOC-V_{OC}$  curve by a linear function, recalling that:

$$V_{oc} = \alpha \cdot SOC + \beta \quad (4.1)$$

That curve is build as example for one cell and shown in Fig. 4.9. Different values of open circuit voltage are recorded in the 5 different SOC ranges. At a given time, open circuit voltage and SOC are measured and then plotted in the same graph. By fitting those data with a linear function in every range, we have a first approximation for  $\alpha$  and  $\beta$ . However, this value is not exact for many reasons. First of all, the open circuit voltage value is not totally accurate, since we waited for about half an hour, and the relaxation phase is not over yet. Secondly, we did not consider the hysteresis effect, which accounts for different open circuit voltage values in charge and discharge phase. We limit ourselves to consider a mean value to make our identification in reasonable time. Also in this case, the initial values are important but not exact, so we give them a small degree of freedom.

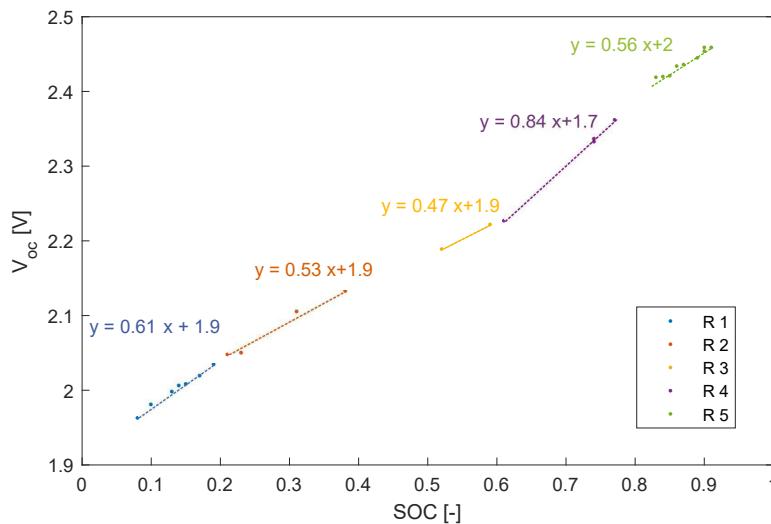


**Fig. 4.9.** Open circuit voltage - state of charge dependence for a generic battery cell: Different colours indicate different ranges. The two coefficients in the equation correspond to the parameters  $\alpha$  and  $\beta$  ( $R$  = range).

A crucial point is also the nominal capacity value  $Q_{nom}$ , which has to be given as known value. As we have seen, the rate capacity effect causes that this value is not constant and it depends on  $C_{rate}$ , SOC and temperature. To have an accurate prediction, we should account for it, but to simplify the model, it is assumed to be constant. The chosen value is the nominal capacity, given by the manufacturer, 16 Ah, at 0.1  $C_{rate}$ . We neglect the capacity dependence

on current intensity and its possible reduction due to ageing phenomena. However, we obtain quite good results also regarding the SOC estimation, as illustrated later. "Quite good results", referring to SOC, have not to be intended in absolute terms, but we mean in comparison to the BMS values. It is the only check we can make with the available devices and techniques in the Microgrid.

Moving to the other parameters, in order to be sure that *greyest* is going to assign the meaning we gave them, we must initialize them properly. Not having any related information, we tried to extract some useful hints looking at the measurements plot. Clearly, it depends on the specific cell one is looking at, but generally it seems that the delayed dynamics last around 200 seconds, the slow ones 20 seconds and the fastest dynamics just few seconds. At this point we have an idea on the time constants values, but still we do not know anything about resistances and capacitances. We tried, randomly, with different values, and finally we choose the more suitable ones. An example of what we obtain at the end of this identification is shown in Tab. 4.1.

$R_1$	$C_1$	$R_2$	$C_2$	$R_3$	$C_3$	$\beta$	$R_0$	$\alpha$	$k_1$	$k_2$	$k_3$	$k_4$	$\sigma$
0.0057	30308	0.002	6293	0.0018	2391	0.817	0.0082	1.77	0.30	-1.24	0.92	0.05	6.97E-06

TABLE 4.1: Estimated parameters relative to one cell at 40-60% SOC

They are relative to one of the most charged cells and valid for a SOC range between 40% and 60%. It is easy to see that the three time constants (the product of resistance and capacitance  $R \cdot C$ ) are 172, 13 and 4 seconds. The variables  $k_1, k_2, k_3$  and  $k_4$  represents the model noise. The small value indicates the model estimation is well done. Also the measurement noise,  $\sigma$  is very small, making that the Kalman filter is going to trust the last measurement a lot.

All the data have been organized in a cell structure, containing 5x2 matrices. The structure contains the name of the SOC range in the first column and 14x13 matrices in the second column, where 14 is the number of estimated parameters corresponding to the cell of the 13 modules. Actually, we have two cell structures, "*cell\_min*", corresponding to the least charged cell per module, and "*cell\_max*", corresponding to the most charged one. The charge comparison is made in terms of voltage, since this value is much more reliable than state of charge. All the cells present similar parameters. They have the same order of magnitude but different values, as a confirmation of the fact that the cells are not identical and they have not the same behaviour under same conditions.

#### 4.2.4 Model simulation

In order to perform model simulations, we need to process our model, converting it from the continuous state-space representation in (3.21) to the discrete form that can be coded in Matlab. In particular, the model is discretized at  $\Delta T = 1$  second resolution. The initial idea, actually, was to have a lower resolution. In effect, within the Commelec Framework all the Microgrid is controlled at 100 ms and this was the initial goal. At the same time, when considering the battery cells, such a low resolution is not affordable for the considerations made in Section 4.1

relative to the limitations of Modbus protocol. However, as we have already seen, the battery dynamics are relatively slow, for example compared to supercapacitors. This should avoid to lose precious information and guarantee the control. On the other hand, since it is physically impossible to go below this limit, we have to accept that  $\Delta T = 1$  s is the best we can achieve.

The discretization is performed using the forward Euler method. The matrices defining the state-space model have different expressions in discrete and continuous system representation. Given the continuous time transition matrix and system input matrices ( $A_c$ ,  $B_c$ ) they become [35]:

$$A = 1 + A_c \Delta T \quad (4.2)$$

$$B = B_c \Delta T \quad (4.3)$$

A first model simulation is performed before implementing the Kalman filter technique, and it is done with the same data used for estimating the parameters and shown in Fig. 4.10, then the model is tested with different data. This first simulation is essentially dedicated to check whether the parameter estimation is accurate enough or not. What we need to perform the simulation is:

- The model, using its state-space form representation by combining (3.21) with (4.2), (4.3) and without including the Kalman Filter gain  $K$ . For the sake of clarity, the model is recalled hereafter in (4.4) and (4.5).

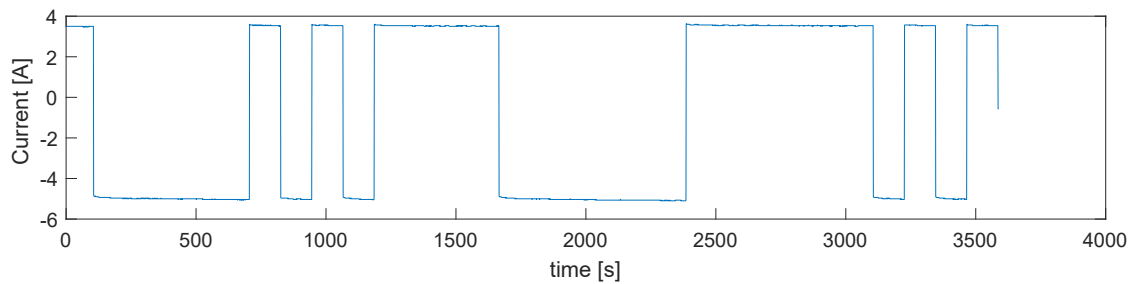
$$\begin{bmatrix} v_{C_1}(t + \Delta T) \\ v_{C_2}(t + \Delta T) \\ v_{C_3}(t + \Delta T) \\ SOC(t + \Delta T) \end{bmatrix} = \begin{bmatrix} 1 - \frac{\Delta T}{R_1 C_1} & 0 & 0 & 0 \\ 0 & 1 - \frac{\Delta T}{R_2 C_2} & 0 & 0 \\ 0 & 0 & 1 - \frac{\Delta T}{R_3 C_3} & 0 \\ 0 & 0 & 0 & 1 \end{bmatrix} \begin{bmatrix} v_{C_1}(t) \\ v_{C_2}(t) \\ v_{C_3}(t) \\ SOC(t) \end{bmatrix} + \begin{bmatrix} \frac{\Delta T}{C_1} & 0 \\ \frac{\Delta T}{C_2} & 0 \\ \frac{\Delta T}{C_3} & 0 \\ \frac{\Delta T}{Q} & 0 \end{bmatrix} \begin{bmatrix} i(t) \\ 1 \end{bmatrix} \quad (4.4)$$

$$V(t + \Delta T) = v_{C_1}(t + \Delta T) + v_{C_2}(t + \Delta T) + v_{C_3}(t + \Delta T) + \beta SOC(t + \Delta T) + R_s i(t + \Delta T) + \alpha \quad (4.5)$$

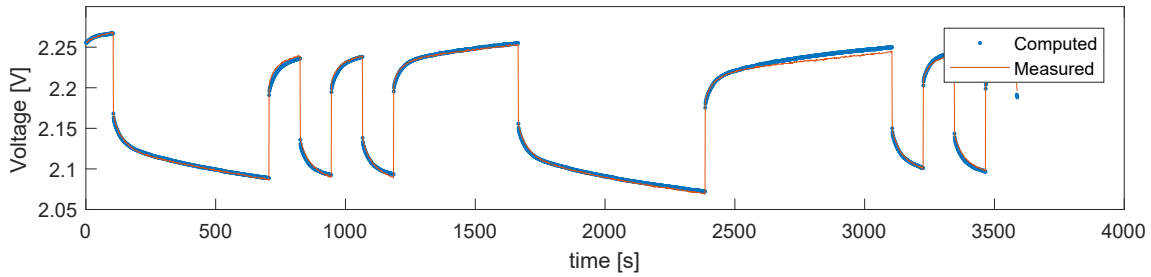
- The current as input. The total battery current is divided by the number of parallel connections  $N_p$  ( $N_p = 3$ ):  $I_{cell} = I_{rack}/3$ . This is not completely true because the cell inconsistency problem affects the cell voltage as well as the current. Without having real measurements and better assumptions, this can be an acceptable hypothesis.
- The estimated parameters.
- The voltage, actual measurement of the model output.
- The internal state initial guess, given in (4.6).

$$x(0) = \begin{bmatrix} v_{C_1}(0) \\ v_{C_2}(0) \\ v_{C_3}(0) \\ SOC(0) \end{bmatrix} = \begin{bmatrix} 0 \\ 0 \\ 0 \\ SOC_m(0) \end{bmatrix} \quad (4.6)$$

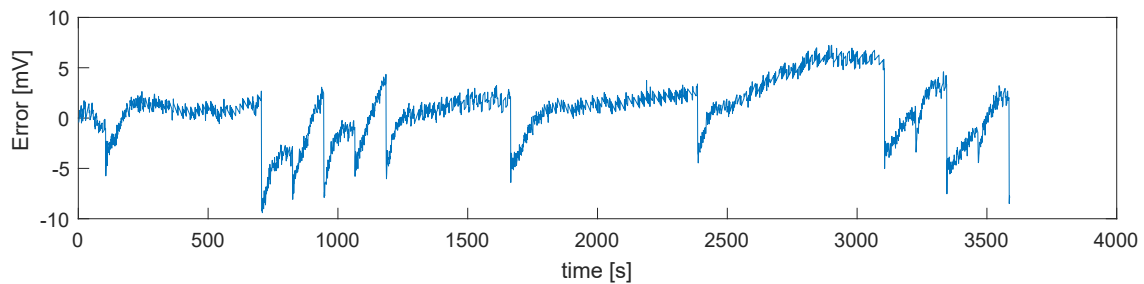
The SOC estimation is included as part of the internal state vector  $x$  within the model to compact the formulations. The results are shown in Fig. 4.10, for the same cell whose parameters are given in Tab. 4.1.



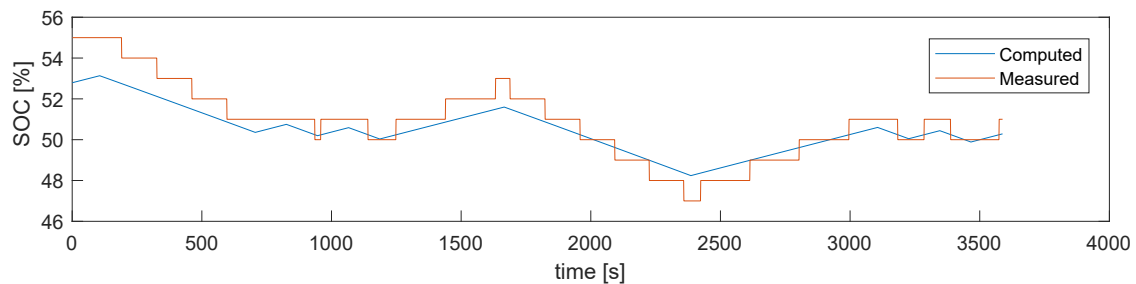
(a) Input current following a PRBS signal.



(b) The red curve is the measured voltage and the blue curve is the approximation given as model output.



(c) Absolute model error, difference between the measured actual voltage and the computed value.



(d) The red curve is the SOC read from the BMS and the blue curve is the computed one with the Amper Hour method.

**Fig. 4.10.** Model simulation results

The results we obtain for these data are very good, confirming that the model is well defined and the parameters properly identified. However, we have to take into account we are in the presence of favourable conditions: the  $C_{rate}$  is exactly the same has been used for the system identification and the SOC range in which these experiments are performed is far from the bounds. It makes that everything is "more predictable", in the sense that there are not weird

non-linearities which are typical of very high or very low state of charge. Therefore, also our assumption about the SOC linearity with the voltage is more precise. All these observations can explain why we do not observe the same very good results in other simulations.

The estimated voltage (blue curve) in Fig. 4.10b is really close to the measured voltage (orange curve). Their absolute difference (Fig. 4.10c) is always lower than 10 mV, it means an error of around 0.4%. From the voltage graph, it appears that the resistance is very good estimated since the voltage drop is practically the same in both real and simulated case. It seems that the biggest committed error occurs concurrently with the current drop. This is due to the fact that, at a given time, the voltage at the next time step is computed using as input the previous current value. It is impossible for the model to predict that after 1 second the current is going to change. The model disturbance is inherently unpredictable.

Since our assumption on the SOC is pretty much correct for those data, the SOC estimation is also very close to the value readed from the BMS (Fig. 4.10d). Clearly, we cannot establish that the Coulomb counting method is totally correct, since a precise criteria of reference does not exist. However, since it needs an initialization which affects a lot the computation, it is always related to the BMS state of charge.

Unfortunately, the voltage simulation for cells at very low or very high SOC is not as accurate as this one, particularly in the range 0-20%. The voltage computed curve is still following the same trend of the measurements, but the difference between the two is not acceptable to correctly control the battery operations.

### Model error

The best way to compare models reliability is to have a metrics based on the error they produce. The error  $e(t)$  is computed in relation to the measured voltage  $V_m(t)$ , by doing the difference between this last item and the voltage predicted  $V_c(t)$  by the model. Then, it is normalized dividing by the most trusted one (measured value), giving  $e_{\%}(t)$ .

$$e(t) = V_m(t) - V_c(t) \quad (4.7)$$

$$e_{\%}(t) = \frac{e(t)}{V_m} \quad (4.8)$$

At this point we obtain a vector of errors, that is not very intuitive to have an overall overview of the model accuracy. Therefore, its root mean square (*rms*) is computed using the Matlab function *rms*. Generally, it is given by:

$$rms = \sqrt{\frac{1}{N} \sum_{k=1}^N |e(t)|^2} \quad (4.9)$$

The results are shown in Fig. 4.11, allowing to make a comparison between the classical TTC model, and the one implemented in this thesis, containing three time constants and the controllable voltage source, linear with the SOC.

Different color indicates different SOC range, while different columns mean different modules, hence, different cells. What is clear from the graphs, is that the error is way lower going

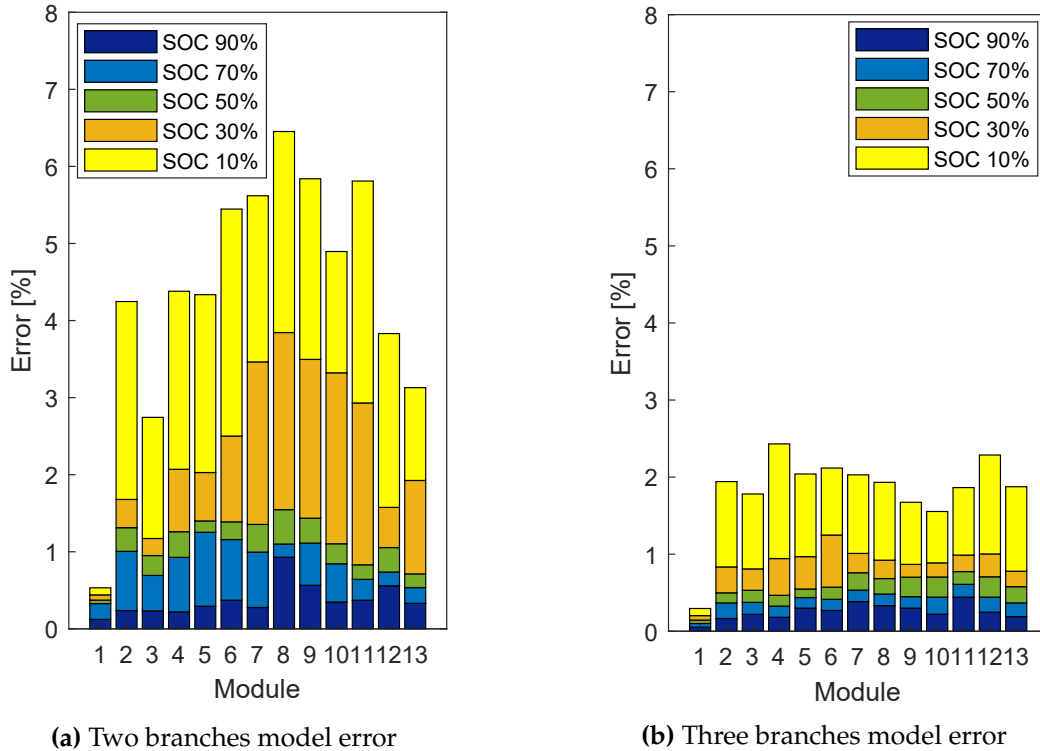


**Fig. 4.11.** Classical two time constant and Modified three time constant model relative errors

from two to three branches. It is incredible how the model is improved just by adding the representation of fastest dynamics and initializing the variables in the right way. However, in both cases, the biggest error occurs in correspondence to the lowest state of charge, although it is still lower than 1.5% in the three time constant model. It is worth noting that the error related to the cell in module 1 is always very small. In effect, from measurements observations one can notice that it is like if this cell was less responding to any kind of stimulation.

If on one hand, the root mean square error is acceptable with some precautions, on the other hand we have to take into account more model failures might occur. The fact that this model simulation is giving such good results, is just a confirmation of the fact that the parameters estimation is well done and the model is accurate for those conditions. Clearly, the model we want to build should be able to represent the cells behavior in all kinds of situations. First of all, we should account for different power values, causing different  $C_{rate}$  and different SOC value. Secondly, one has to consider probable accumulation errors and any other kind of faults. For all these reasons, the Kalman filter technique incorporation is essential.

#### 4.2.5 Model implementation using Kalman-filtering technique

As already stated, Kalman Filter technique is able to update the model output, considering the last available measurement. Such a technique, is able to follow all sorts of trend. In some cases the voltage behaviour is completely abnormal and very difficult to model. For instance, in Fig. 4.12 the highest value of voltage per module is shown.

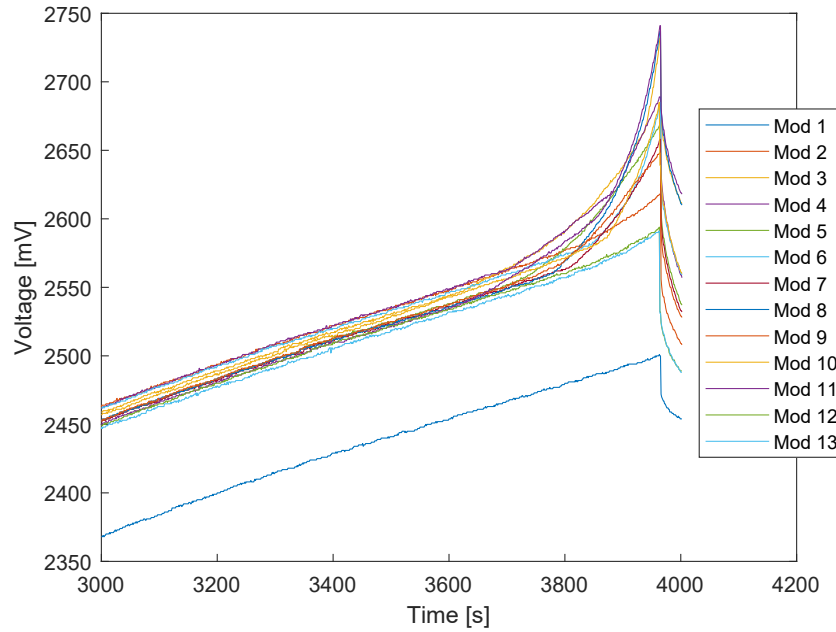


Fig. 4.12. Data registered while charging the battery with a power of 20 kW.

These data have been taken by charging the battery with a constant power of 20 kW, with an average current per cell of 10 A. Technical data for each cell given by the manufacturer are shown in Table 4.2. It is clear that some of the cells in Fig. 4.12 are out of the suggested threshold.

Maximum voltage	2.7 V
Minimum voltage	1.7 V
Maximum charge current	64 A
Minimum discharge current	64 A

TABLE 4.2: Cell technical data

Testing the identified model for the cells in critical conditions with these data, it does not appear to be adequate. Especially with reference to the cells with very high voltage values, the model is not able to follow their characteristic trend.

For introducing the Kalman filter method within our model, we need to write the Kalman gain, representing process and measurement noise, in a discrete way. This is done by following the procedure illustrated in [35], obtaining (4.10), (4.11), (4.12).

$$K = M_1 M_2^T \quad (4.10)$$

where  $M_1$  and  $M_2$  are given according to the Van Loan's method [50] and are matrix exponentials, which are approximated by the first order truncation of their respective Taylor expansions:

$$M_1 = e^{H_c \Delta T} = 1 + H_c \Delta T \quad (4.11)$$

$$M_2 = e^{A_c^T \Delta T} = 1 + A_c^T \Delta T \quad (4.12)$$

By simulating the model including the Kalman filtering technique, the computed voltage is following the measurements perfectly. The results for two of the most charged cells (in Module 3 and 11) are shown in Fig. 4.13 for both models, with and without Kalman Filter. The orange curves are the actual values of voltages, while the blue dashed lines represent the model prediction output. We can see that in the model without Kalman Filter (Fig. 4.13a) the voltage prediction is still quite good until 2.6 V is reached, but then it completely underestimates the value. The broken line at around 3700 seconds is due to the fact that, changing the SOC between two subsequent moments, the parameters are different and so is the model. The computed value of voltage is always within the allowed range, although the real value is not. This is clearly non-acceptable for correctly operating this device, that is why Kalman Filter can help. In fact, in Fig. 4.13b, the results for the same cells simulating the complete model are displayed. In this case it is able to follow the voltage trend properly.

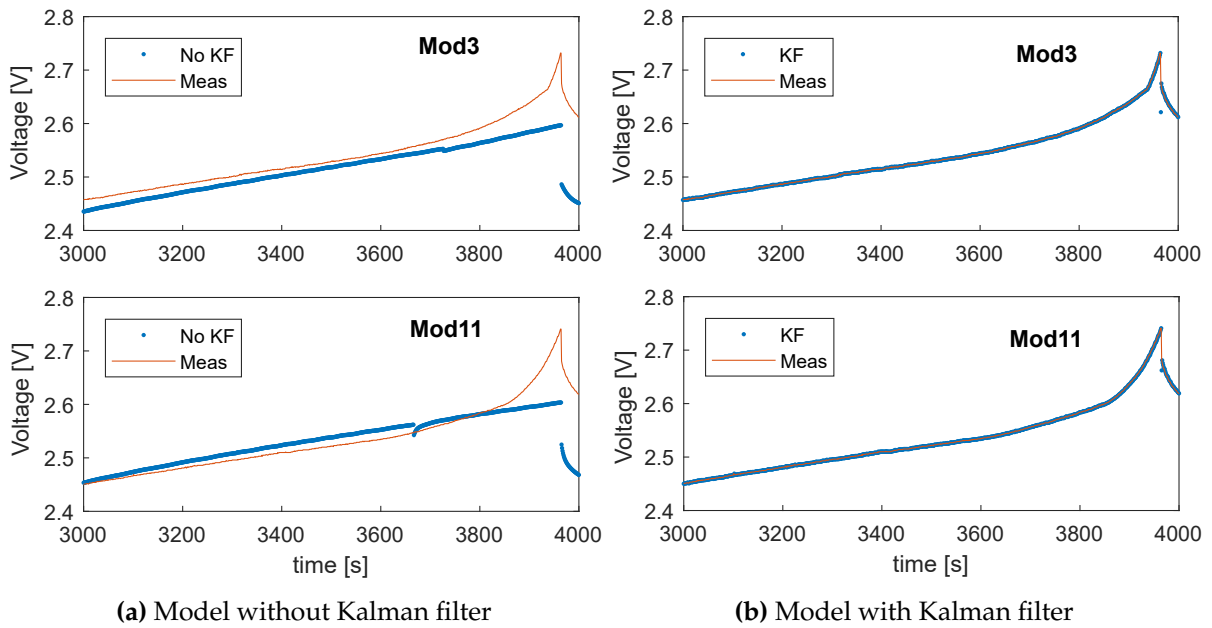
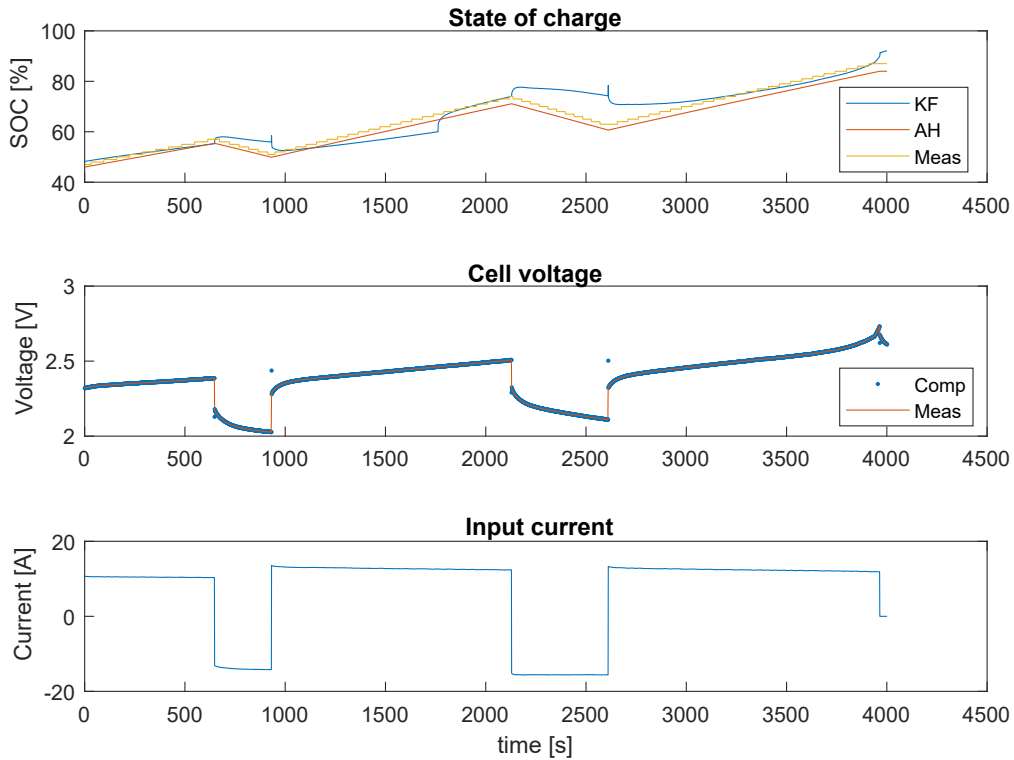


Fig. 4.13. Model simulation without and with Kalman filter

The main advantage is that at each iteration the internal state  $x$  is updated using the past information. This leads to better results, able to predict the short-term evolution, adjusting the internal state at each iteration. The whole data taken in the same experimental session, are represented in Fig. 4.14 for the cell in module 3.

The current corresponds to a power equal to 20 kW, as before. The predicted cell voltage (blue curve) follows the real trend (orange curve) very well. It is possible to notice that there



**Fig. 4.14.** Kalman filter technique based model

are some points where the estimates are wrong. They are in correspondence of the sign change of the current (passing from charge to discharge and vice versa). However, it is worth noting that the model converges quickly. What should be mentioned is also the SOC estimation. The yellow line is the value measured from the BMS, the orange one is estimated by the Coulomb Counting method (indicated as AH, Ampere Hour method), and the blue curve is extrapolated from the internal state corrected by the Kalman Filter. In some points the three of them are superposed, while in some cases the blue curve is not very accurate. At time  $t = 2300$  s, the SOC increases while we are discharging and this is clearly not possible. It would suggest that the Coulomb counting method works better than the value we get from the state space model using Kalman filter.

#### 4.2.6 Maximum power flexibility computation

The maximum power flexibility consists in finding the maximum charge and discharge power which make the battery stay within its (or cells) limits for a given initial state. It relies on the procedure derived in Section 3.2.2 and Section 3.2.3. It is firstly computed at the cell level and then translated to the whole battery array through the current. In this respect, first of all, the maximum charge power is computed for the most charged cell and the maximum discharge power for the most discharged cell. Sometimes we refer to maximum and minimum power. It has to be noted that this notation derives from the sign convention of power and current used by the BMS. They represent:

- $P_{max}$  the maximum allowed (positive) power, that serves to charge, by ensuring that the highest voltage is lower than (or equal to) 2.7 V.
- $P_{min}$  is the minimum power, negative, used to discharge the battery by staying within the limits (minimum voltage is always higher of equal 1.7 V).

The computation is made in the Matlab script "*Cell\_limiting\_power.mat*". The power limits are computed separately for the two modes, where we have to distinguish current and voltage constraints, identifying the most conservative one. More details on the script are given in Appendix A. The limits imposed in the two following simulations are more restrictive than the real ones:  $I_{max} = 14$  A,  $I_{min} = -14$  A,  $V_{max} = 2.6$  V,  $V_{min} = 1.8$  V.

### Result for charging mode at cell level

The data have been taken by charging and discharging randomly the battery on August 6th. The measurements have been analysed and the maximum power computed. The results are shown in Fig. 4.15.

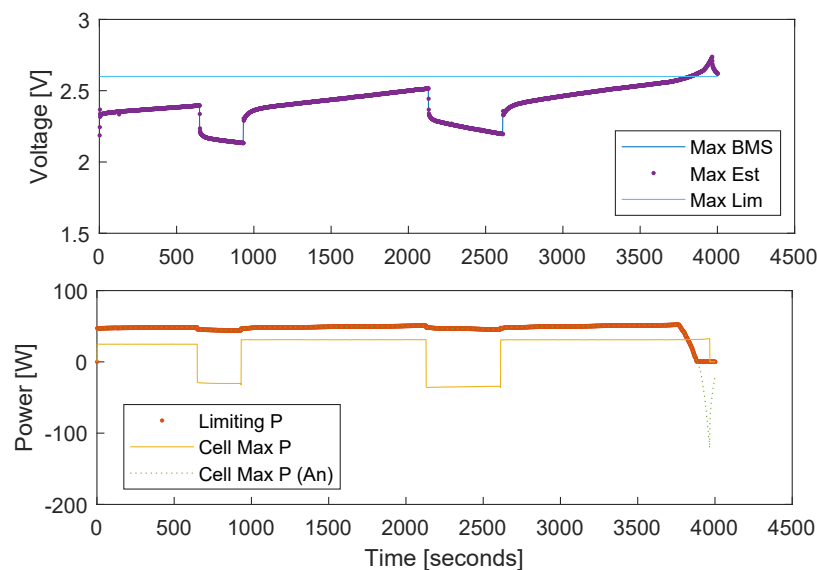


**Fig. 4.15.** Maximum limiting power

What we have to focus on is the violet curve, representing the maximum voltage, and the red curve, representing the maximum allowed power. Globally, the results are quite promising. In fact, it can be clearly seen that as soon as the voltage is going closer to the limit, the maximum power (red curve) starts to decrease. When the voltage (violet curve) reaches the upper limit, the maximum power becomes smaller than the actual cell power (the red curve goes below the yellow line). Furthermore, with the increment of the voltage, already out of the bound, the maximum power continues to decrease, until it reaches 0 kW. All the values different from zero, with the voltage higher than 2.6 V, correspond the value which keeps the voltage equal to the limit value.

In effect, looking at the global rack, we cannot see these dynamics, and we are still charging when the considered cell is already overcharged. After the peak value has been reached, the voltage starts to decrease because the battery security system has been activated. If we used our model, we would have been able to use the battery without disruption in a more appropriate way.

**Result for discharging mode at cell level**

In discharging mode, the lowest voltage in absolute terms is considered. The data are relative to August 10th, with the battery subjected to intentional random charge/discharge phases. The results are shown in Fig. 4.16. The yellow curve, is the real voltage behavior regarding the least charged cell. Continuing to discharge the battery, at some point, it crosses the permitted limit value (green line). The violet curve is the actual cell power, and the blue curve represents the minimum computed power, namely the limit we should not cross to respect cell limits. Also in this case, the blue curve decreases (in absolute terms) as soon as the voltage approaches the limit value, until it is exactly equal to 1.8 V. At this point, the blue curve crosses the violet curve, indicating that the discharging power has to decrease immediately.

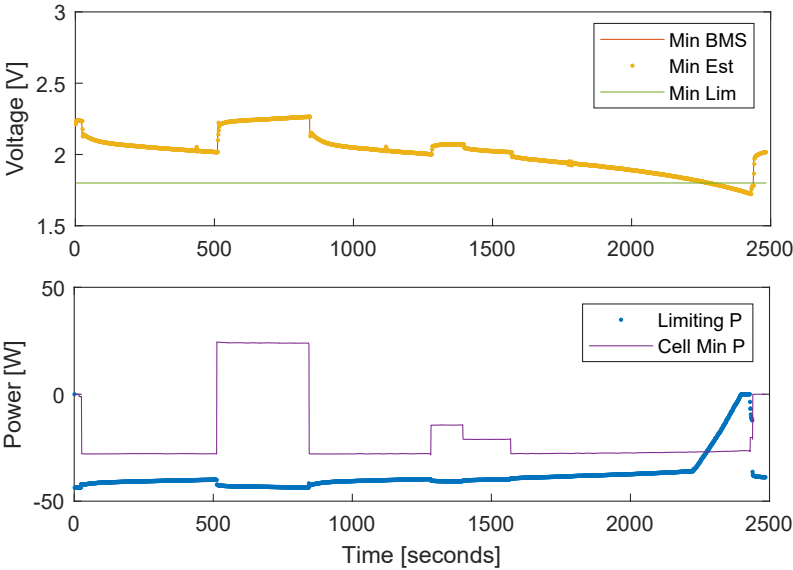


**Fig. 4.16.** Maximum limiting power

It is true that the BMS acts at some time by shutting down the system. However, it occurs after the limits are exceeded already for few seconds and it requires to be restarted by hand. This means that we have to limit the power before interruption of service occurs and irreversible damages to the cell material take place.

### 4.3 Experimental validation with the stack in the microgrid

The real-time validation has to be done by using real time measurements to compute the power limits with the model. Since the measurements are available in the LabVIEW project and the model was only coded in Matlab, we had two options:

1. Get measurements from the battery directly on the MATLAB code
2. Code the whole model in LabVIEW.

This second options has been chosen since it is really difficult to create a communication between the two softwares. A new VI *power limits.vi* has been created and added to the original project. A piece of the global code is given in Appendix A.2. It reads all the measurements in real-time at 1 second resolution, giving as output the prediction for the next time time, after 1 second, in terms of voltage for the two most crical cells. It is constituted by several blocks and subVIs, which aim to perform the following steps. The algorithm is presented in Fig. 4.17. They are given for the most charged cell limiting power, but for the least charged one we do exactly the same:

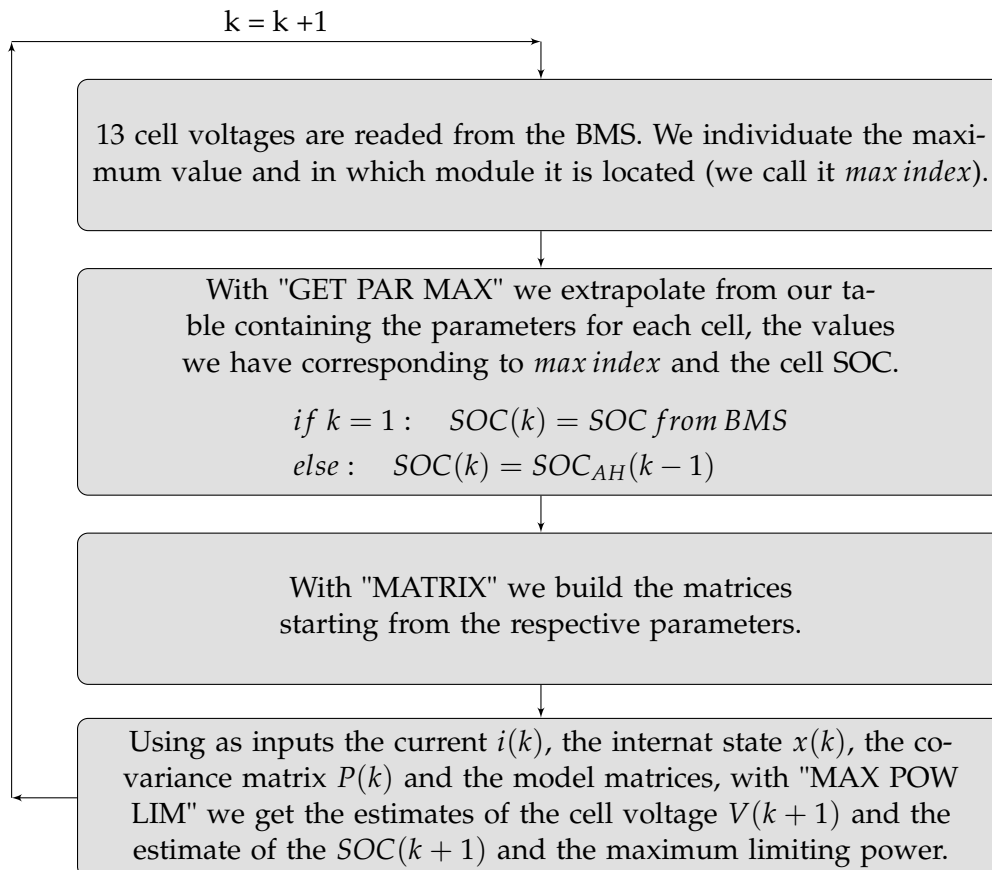


Fig. 4.17. Voltage prediction and maximum power flexibility computation in the LabVIEW project

1. All the 13 cells voltages are readed from the BMS. We individuate the maximum value and in which module it is located (we call it *max index*).

2. With "GET PAR MAX" we extrapolate from our table containing the parameters for each cell, the values we have corresponding to *max index* and the cell SOC. The SOC value is the one readed by the BMS at the first iteration, and the one computed with the Coulomb counting method later.
3. With "MAT RIX" we build the matrices from the respective parameters.
4. Using the input  $u(k) = [i(k) \quad 1]^T$  and the internat state  $x(k)$ , the covariance matrix  $P(k)$  and the model matrices, with "MAX POW LIM" we get the estimates of the cell voltage at time  $(k+1)$  and the estimate of the SOC with Kalman Filter. In the same subVI, with the predicted voltage  $V(k+1)$  and the actual current  $i(k)$ , voltage and current bounds, the maximum limiting power is computed.
5. The results are shown in the front panel, and can be logged, together with other measurements, in TDMS files.
6. It is repeated continuously in a while loop that can be stopped with a user external command through appropriate "STOP" button.

The same procedure is repeated for the minimum limiting power. The limits imposed in the model are very restrictive:  $1.7 V < v_{cell} < 2.7 V$  and  $-14 A < i_{cell} < 14 A$ .

Actually, also a second simplified version of this model has been created. It uses only one set of parameters for all the cells, instead of 26. It can be directly applied, without finding where the crical cells are and the related parameters. The SOC dependence is still taken into account, having 5 different sets of matrices depending on the SOC, but they do not depend on the particular cell. It assumes all the cells can be represented with the same exact model, found as an average of all the other parameters. The data have been registered for both models, and shown in next paragraphs.

### **Result for 2018.08.27**

The experimental session starts with the battery at high SOC, in relaxation phase, with the voltage decreasing very slowly. Suddenly, we start to charge the battery, with a power of 20 kW. In less than 10 minutes the voltage gets closer to the limit. We start to decrease the power, accordingly to the value of computed limiting power, step by step. Such a value, makes that the voltage stays very close to the limit, without exceeding it. Then, we stop charging for a while (intentionally, no forced shut down occurred). After some random charge/discharge cycles, we incur to limit values again. The same procedure as before is repeated: the power is reduced according to the limiting computed value. The SOC estimaton is given with the Coulomb counting method, and is very similiar to the BMS value, although this last one presents some "jumps". It can be an estimation error on the BMS side, or it is due to the fact that the critical chell has changed. It is worth noting that both models (using 26 sets or 1 set of parameters) give roughly the same results. This can be explained thinking about the power of Kalman filtering technique.

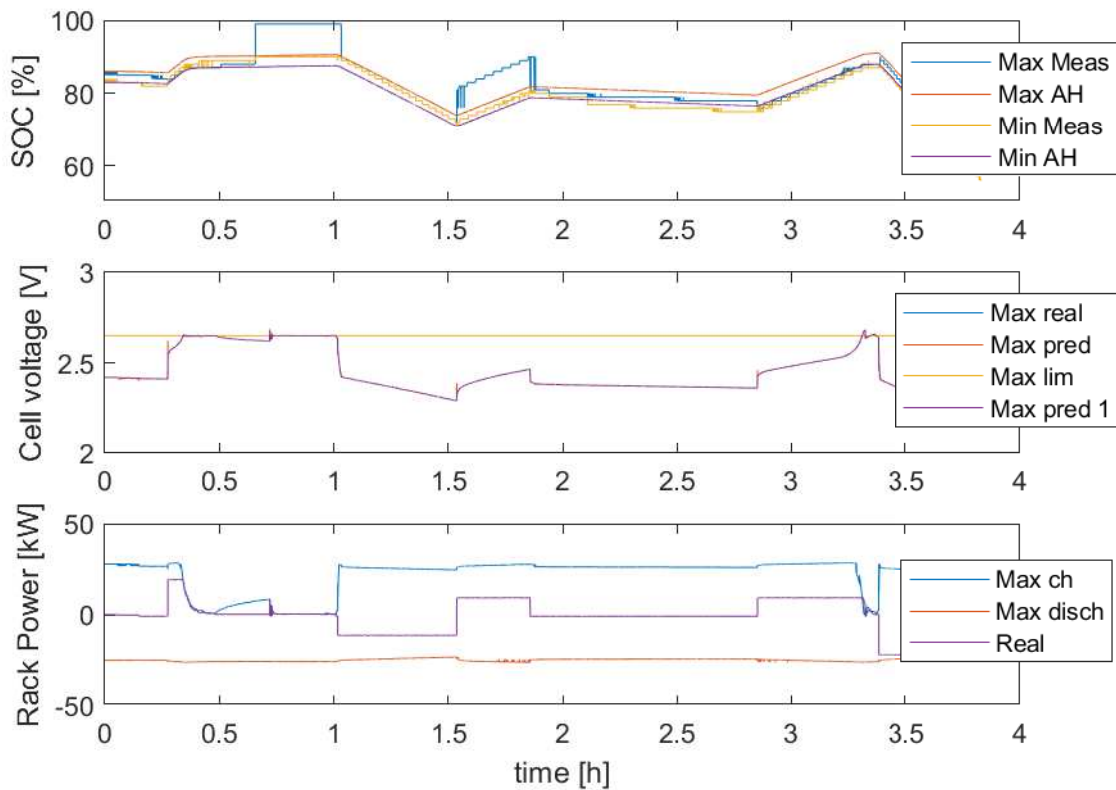


Fig. 4.18. Results for 2018.08.27

### Result for 2018.08.29

These results in Fig. 4.19 show that also the minimum limiting power is well estimated. In the voltage plot, we can see that in the first 30 minutes the cell voltage (blue curve) is far from the limit value, therefore the maximum discharge power (red curve) is much higher than the one real one (violet curve, is basically zero). When we start discharging, the voltage decreases. At the same time, we reduce the maximum discharge power, in accordance with the value computed by our model. Soon the cell voltage reaches the lower limit. At this time, we keep extracting the maximum value of allowed power, and the voltage remains constant and equal to the minimum value. The maximum charge power is almost constant, since we are far from the upper bound of the voltage, hence there is no reason to decrease.

The values of power which allow to stay within the imposed limits of voltage and current at the cell level are in the area between the maximum charge and discharge power: the blue and the red curve.

The SOC estimation is also quite good estimate since it is very close to the measured values.

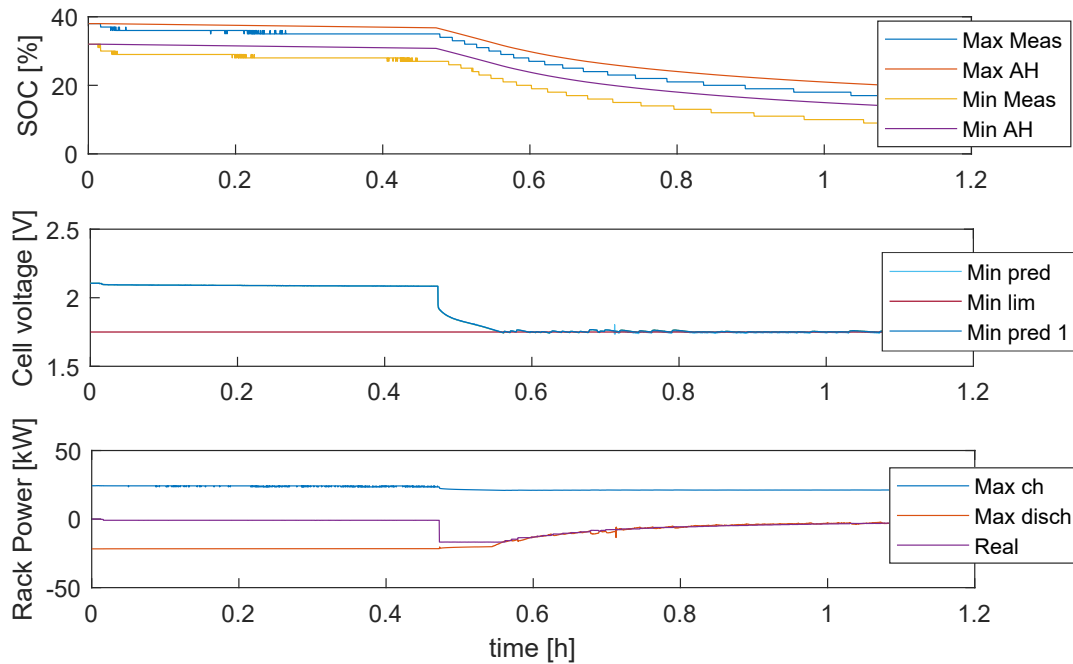


Fig. 4.19. Results for 2018.08.29

## 4.4 Discussion

In Fig. 4.18 and Fig. 4.19 is clearly visible the meaning of the maximum power flexibility. In the third plot of both figures, all the values of power included between the red and the blue curves are acceptable, in the sense that all the cells limits are not violated. The error we commit by using the simplified model with 1 set of parameters or the complete model with 26 sets of parameters is approximately the same and shown in Fig. 4.20:

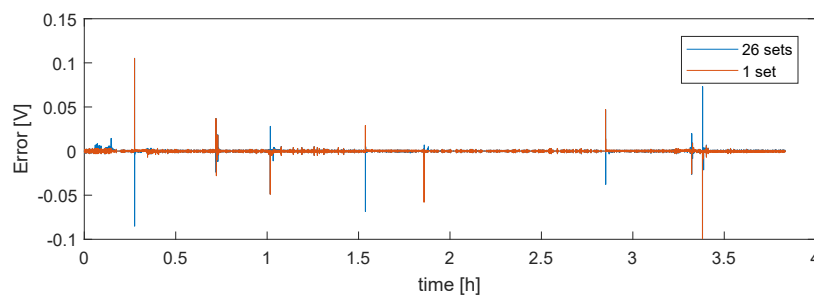


Fig. 4.20. Absolute error comparison using 1 set or 26 sets of parameters

The maximum error occurs always at the same instant. Its value and (often) the sign change, due to the filter action. The parameters of both models are not the "real" ones, because as we have seen they should change according to  $C_{rate}$ , temperature, SOC, but this is not possible in real-time applications. Using the filter, it accounts for the error we commit using constant parameters by modifying the system internal state (which is not always true). The behaviour of the blue and the red curves in Fig. 4.20 is slightly different, especially where the current value changes, because is there that our model gives large errors. For instance, the first big error

occurs after about 20 minutes the experimental session started, when we are charging at high power. The model output in this case is wrong, and the error, 0.1 V in absolute terms, is not negligible (4%). The prediction is made with the previous current value and it does not expect the current will change after 1 second. The same idea is still valid for the other points where the error is significant.

The grey-box models available in literature are quite easily to implement. However, as we have seen, even if the estimation is very accurate, the nonlinear phenomena cannot be easily generalized. Thanks to the Kalman filter, we are able to correct these inaccuracies. It acts on correcting the system internal state with the last available measurements, taking into account model error and measurement noise. However, when the parameters are not very good estimated, the internal state meaning is lost. That is why the SOC estimated with the Kalman filter technique is not always very precise.

## Chapter 5

# Conclusion

The thesis shows the problematic of the correct use of batteries, which is in general assolved by a dedicated system: the battery management system (BMS). Experimental observations show that it is not able to control and keep all the cells of a battery pack within voltage and current constraints. The implemented model is able to limit the battery operations by monitoring the most critical cell values. It predicts the battery cell response for a given input to estimate the boundary conditions, in a way that the operational limits of the cells are not exceeded. The predictor model is based on grey-box modeling, relying on equivalent electric circuit where physical knowledge and abstract representation are mixed. Although the model has been augmented compared to the classical two time constant model, without any adjustment, it is not sufficient to describe non linear features such as voltage dependency on SOC,  $C_{rate}$ , temperature. The constant temperature assumption results quite accurate. All the other issues, have been settled by using Kalman filter, a recursive method able to update the estimates with the last measurement. The model is finally able to follow the real voltage measurements, giving very low prediction errors. The results obtained are used to compute, at every moment, the maximum limiting power. It is given as a function of the maximum and minimum voltage and current limits, and depends on some of the model parameters as well: series resistance, open circuit voltage, internal state, voltage prediction and actual current. Both the cell-based battery model and the predictor model have been completely defined for a 25 kW / 25 kWh battery connected to the experimental EPFL Microgrid, and then implemented into a microcontroller responsible to control the battery. The obtained results are characterized by a quality such that they can be directly used by the battery operator without further adjustments.

Actually, two models have been implemented running at the same time. The only difference is that one considers a different set of parameters for every monitored cell, while the other one is using only one set for all the cells, which is given by an average of all of them. The experimental results show that their voltage prediction is slightly different. Considering the effort to completely identify the model parameters, based on those results, one can think to use the same parameters for all the cells. This is due to the powerful ability of the Kalman filter, but it is accompanied by a lost of the physical meaning of the internal state. In effect, using parameters that are not well estimated will give large errors in the SOC estimation. It is for that reason that, especially close to the limit conditions, the SOC is better estimated with the Coulomb conting method rather than the value obtained using the Kalman filter technique.

The state of charge estimation is still a crucial point. Although it is quite accurate with the

Coulomb counting method, it requires an initial value which should be improved. Currently, it is taken from the BMS measurements. What one can do, is to have a "hybrid model" between Coulomb counting method and look up tables based on open-circuit voltage technique. The initial value can be taken from the table when the battery is in resting phase, so that the relaxation phase can be considered over and the voltage close to open circuit condition. Then, the effectively charge exchanged can be easily computed with the Coulomb counting method. A possible future work could be the study of a model able to account for the charge effectively available in the cells. In effect, the only certain way to know the available remaining charge at a given  $C_{rate}$  is to discharge completely the battery and measure the extracted charge, but it requires several slow and tricky measurements.

## Appendix A

# Maximum power flexibility computation

### A.1 Matlab script

For the charge phase we have:

```
% voltage constraints
max_vP = @(V) (1/max_Rs)* V^2 - ((maxC * max_x + max_alpha)/max_Rs) * V;
max_vPmax = max_vP(Vmax);

% current constraints
max_iP = @(i) max_Rs * i^2 + (maxC * max_x + max_alpha) * i;
max_iPmax = max_iP(Imax);
Pmax(kk+1) = min(max_vPmax, max_iPmax);
```

The power limit for the discharge phase is computed as:

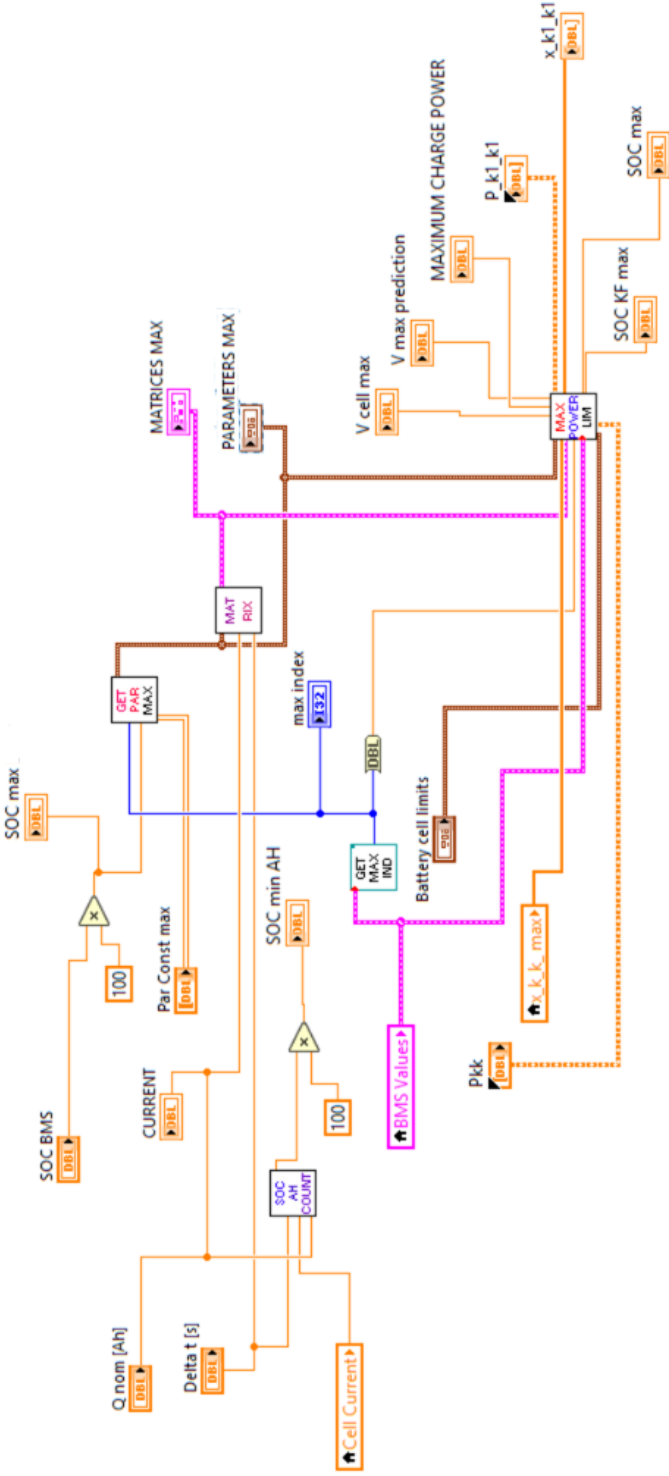
```
% voltage constraints
min_vP = @(V) (1/min_Rs)* V^2 - ((minC * min_x + min_alpha)/min_Rs) * V;
min_vPmin = max(min_vP(Vmin), min_vP((minC*min_x + min_alpha)/2));

% current constraints
min_iP = @(i) min_Rs * i^2 + (minC * min_x + min_alpha) * i;
min_iPmin = max(min_iP(Imin), min_iP(-(minC*min_x + min_alpha)/(2 * min_Rs)));
Pmin(kk+1) = max(min_vPmin, min_iPmin);
```

And finally the limiting current is derived from the power, dividing by the cell voltage:

```
I_Pmax(kk+1,1) = Pmax(kk+1)/maxVoltage;
I_Pmin(kk+1,1) = Pmin(kk+1)/minVoltage;
```

## A.2 LabVIEW code



# Bibliography

- [1] Andrey Bernstein et al. "A composable method for real-time control of active distribution networks with explicit power setpoints. Part I: Framework". In: *Electric Power Systems Research* 125 (2015), pp. 254–264.
- [2] MEV Team et al. "A guide to understanding battery specifications". In: (2008).
- [3] Lennart Ljung. "System Identification". In: *Signal Analysis and Prediction*. Ed. by Ales Procházka et al. Boston, MA: Birkhäuser Boston, 1998, pp. 163–173.
- [4] Lennart Ljung. *System identification : theory for the user*. eng.
- [5] Gholam-Abbas Nazri and Gianfranco Pistoia. *Lithium batteries: science and technology*. Springer Science & Business Media, 2008.
- [6] James F Manwell and Jon G McGowan. "Lead acid battery storage model for hybrid energy systems". In: *Solar Energy* 50.5 (1993), pp. 399–405.
- [7] Maryam Bahramipanah. "Advanced Control of Active Distribution Networks Integrating Dispersed Energy Storage Systems". PhD thesis. École Polytechnique Fédérale de Lausanne, 2016.
- [8] Debashis Panigrahi et al. "Battery life estimation of mobile embedded systems". In: *VLSI Design, 2001. Fourteenth International Conference on*. IEEE. 2001, pp. 57–63.
- [9] *LecCell 30Ah High Energy*. 936C08-B01-G004. Leclanché. May 2014.
- [10] Zhile Yang et al. "A new self-learning TLBO algorithm for RBF neural modelling of batteries in electric vehicles". In: *Evolutionary Computation (CEC), 2014 IEEE Congress on*. IEEE. 2014, pp. 2685–2691.
- [11] Cheng Zhang et al. "Battery modelling methods for electric vehicles-A review". In: *Control Conference (ECC), 2014 European*. IEEE. 2014, pp. 2673–2678.
- [12] Carmelo Speltino et al. "Experimental identification and validation of an electrochemical model of a lithium-ion battery". In: *Control Conference (ECC), 2009 European*. IEEE. 2009, pp. 1053–1058.
- [13] K. A. Smith, C. D. Rahn, and C. Wang. "Model-based electrochemical estimation of lithium-ion batteries". In: *2008 IEEE International Conference on Control Applications*. 2008, pp. 714–719.
- [14] Marc Doyle, Thomas F Fuller, and John Newman. "Modeling of galvanostatic charge and discharge of the lithium/polymer/insertion cell". In: *Journal of the Electrochemical Society* 140.6 (1993), pp. 1526–1533.

- [15] Thomas F. Fuller, Marc Doyle, and John Newman. "Simulation and Optimisation of the Dual Lithium Ion Insertion Cell". In: 141 (Jan. 1994), pp. 1–10.
- [16] Tae-Kyung Lee. "Development and implementation of control-oriented electrochemical battery models in a battery management system". In: *American Control Conference (ACC), 2015*. IEEE. 2015, pp. 717–722.
- [17] C. Zhang, Z. Yang, and K. Li. "Modeling of Electric Vehicle batteries using RBF neural networks". In: *2014 International Conference on Computing, Management and Telecommunications (ComManTel)*. 2014, pp. 116–121.
- [18] Wen-Yeau Chang. "Estimation of the state of charge for a LFP battery using a hybrid method that combines a RBF neural network, an OLS algorithm and AGA". In: *International Journal of Electrical Power & Energy Systems* 53 (2013), pp. 603–611.
- [19] Min Chen, Gabriel A Rincon-Mora, et al. "Accurate electrical battery model capable of predicting runtime and IV performance". In: *IEEE transactions on energy conversion* 21.2 (2006), pp. 504–511.
- [20] Z. M. Salameh, M. A. Casacca, and W. A. Lynch. "A mathematical model for lead-acid batteries". In: *IEEE Transactions on Energy Conversion* 7.1 (1992), pp. 93–98.
- [21] C-J Zhan et al. "Two electrical models of the lead-acid battery used in a dynamic voltage restorer". In: *IEE Proceedings-Generation, Transmission and Distribution* 150.2 (2003), pp. 175–182.
- [22] Domenico Di Domenico, Giovanni Fiengo, and Anna Stefanopoulou. "Lithium-ion battery state of charge estimation with a Kalman filter based on a electrochemical model". In: *Control Applications, 2008. CCA 2008. IEEE International Conference on*. Ieee. 2008, pp. 702–707.
- [23] Yao He et al. "A new model for State-of-Charge (SOC) estimation for high-power Li-ion batteries". In: *Applied Energy* 101 (2013), pp. 808–814.
- [24] Jürgen Garche, Andreas Jossen, and Harry Döring. "The influence of different operating conditions, especially over-discharge, on the lifetime and performance of lead/acid batteries for photovoltaic systems". In: *Journal of Power Sources* 67.1-2 (1997), pp. 201–212.
- [25] Kong Soon Ng et al. "Enhanced coulomb counting method for estimating state-of-charge and state-of-health of lithium-ion batteries". In: *Applied energy* 86.9 (2009), pp. 1506–1511.
- [26] Gregory L Plett. "Extended Kalman filtering for battery management systems of LiPB-based HEV battery packs: Part 3. State and parameter estimation". In: *Journal of Power sources* 134.2 (2004), pp. 277–292.
- [27] Flavio B Vidal and Victor H Casanova Alcalde. "Object Visual Tracking Using Window-Matching Techniques and Kalman Filtering". In: *Kalman Filter*. InTech, 2010.
- [28] Mouna Ghanai and Kheireddine Chafaa. "Kalman Filter in Control and Modeling". In: *Kalman Filter*. Ed. by Vedran Kordic. Rijeka: IntechOpen, 2010. Chap. 2.
- [29] Harold W Sorenson. "Least-squares estimation: from Gauss to Kalman". In: *IEEE spectrum* 7.7 (1970), pp. 63–68.

- [30] Wikipedia contributors. *Kalman filter* — *Wikipedia, The Free Encyclopedia*. [Online; accessed 18-September-2018]. 2018. URL: [https://en.wikipedia.org/w/index.php?title=Kalman\\_filter&oldid=859052165](https://en.wikipedia.org/w/index.php?title=Kalman_filter&oldid=859052165).
- [31] Fernando P. Marafao et al. "Kalman Filter on Power Electronics and Power Systems Applications". In: *Kalman Filter*. Ed. by Victor M. Moreno and Alberto Pigazo. Rijeka: IntechOpen, 2009. Chap. 17.
- [32] M. H. A Davis. *Stochastic Modelling and Control*. eng.
- [33] Seongjun Lee et al. "State-of-charge and capacity estimation of lithium-ion battery using a new open-circuit voltage versus state-of-charge". In: *Journal of Power Sources* 185.2 (2008), pp. 1367–1373. URL: <http://www.sciencedirect.com/science/article/pii/S0378775308017965>.
- [34] Chia-Nan Ko and Cheng-Ming Lee. "Short-term load forecasting using SVR (support vector regression)-based radial basis function neural network with dual extended Kalman filter". In: *Energy* 49 (2013), pp. 413–422. ISSN: 0360-5442.
- [35] Sossan Fabrizio et al. "Achieving the dispatchability of distribution feeders through prosumers data driven forecasting and model predictive control of electrochemical storage". In: *IEEE Transactions on Sustainable Energy* 7.4 (2016), pp. 1762–1777.
- [36] M. Verhaegen and P. Van Dooren. "Numerical aspects of different Kalman filter implementations". In: *IEEE Transactions on Automatic Control* 31.10 (1986), pp. 907–917.
- [37] Simon Haykin. *Kalman filtering and neural networks*. Vol. 47. John Wiley & Sons, 2004.
- [38] Emil Namor et al. "Experimental Assessment of the Prediction Performance of Dynamic Equivalent Circuit Models of Grid-connected Battery Energy Storage Systems". In: (2018), p. 6.
- [39] Niels Rode Kristensen and Henrik Madsen. "Continuous time stochastic modelling". In: *Mathematics Guide* (2003), pp. 1–32.
- [40] Niels Rode Kristensen, Henrik Madsen, and Sten Bay Jørgensen. "Parameter estimation in stochastic grey-box models". In: *Automatica* 40.2 (2004), pp. 225–237.
- [41] Mohit Bansal. *Denoising of Speech and ECG Signal by Using Wavelets: Digital Signal Processing*. Sept. 2012.
- [42] Vedran Bobanac et al. "Laboratory for Renewable Energy Sources and Identification of the Laboratory Wind Turbine Model". In: *Proceedings of the 18th International Conference on Process Control, Slovakia*. 2011.
- [43] AJ Fairweather, MP Foster, and DA Stone. "Battery parameter identification with pseudo random binary sequence excitation (prbs)". In: *Journal of Power Sources* 196.22 (2011), pp. 9398–9406.
- [44] Xianzhi Gong, Rui Xiong, and Chris Mi. "Study of the Characteristics of Battery Packs in Electric Vehicles With Parallel-Connected Lithium-Ion Battery Cells". In: 51 (Mar. 2014), pp. 1–1.

- [45] Rui Xiong et al. "Adaptive state of charge estimator for lithium-ion cells series battery pack in electric vehicles". In: *Journal of power sources* 242 (2013), pp. 699–713.
- [46] J. Cao, N. Schofield, and A. Emadi. "Battery balancing methods: A comprehensive review". In: *2008 IEEE Vehicle Power and Propulsion Conference*. 2008, pp. 1–6.
- [47] M. Bahramipanah et al. "An adaptive model-based real-time voltage control process for Active Distribution Networks using Battery Energy Storage Systems". In: *2016 Power Systems Computation Conference (PSCC)*. 2016, pp. 1–8.
- [48] M. Bahramipanah et al. "A Decentralized Adaptive Model-Based Real-Time Control for Active Distribution Networks Using Battery Energy Storage Systems". In: *IEEE Transactions on Smart Grid* 9.4 (2018), pp. 3406–3418.
- [49] *Slave Interface Description*.
- [50] C. Van Loan. "Computing integrals involving the matrix exponential". In: *IEEE Transactions on Automatic Control* 23.3 (1978), pp. 395–404.